Article

Structural and Spectroscopic Studies on Pt···Pt and π–π Interactions in Luminescent Multinuclear Cyclometalated Platinum(II) Homologues Tethered by Oligophosphine Auxiliaries

Wei Lu, Michael C. W. Chan, Nianyong Zhu, Chi-Ming Che, Chuannan Li, and Zheng Hui

J. Am. Chem. Soc., **2004**, 126 (24), 7639-7651• DOI: 10.1021/ja039727o • Publication Date (Web): 28 May 2004

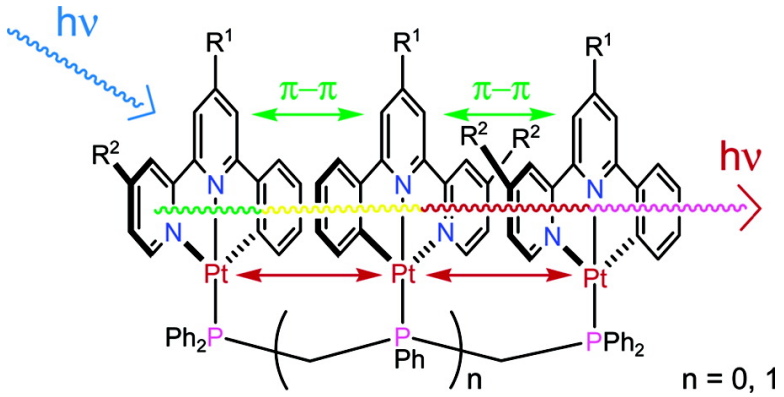

More About This Article

Additional resources and features associated with this article are available within the HTML version:

- Supporting Information
- Links to the 16 articles that cite this article, as of the time of this article download
- Access to high resolution figures
- Links to articles and content related to this article
- Copyright permission to reproduce figures and/or text from this article

View the Full Text HTML

J|A|C|S
ARTICLES
Published on Web 05/28/2004

Structural and Spectroscopic Studies on Pt···Pt and $\pi-\pi$ Interactions in Luminescent Multinuclear Cyclometalated Platinum(II) Homologues Tethered by Oligophosphine Auxiliaries

Wei Lu, Michael C. W. Chan, Nianyong Zhu, Chi-Ming Che,* Chuannan Li, and Zheng Hui

Contribution from the Department of Chemistry and HKU-CAS Joint Laboratory on New Materials, The University of Hong Kong, Pokfulam Road, Hong Kong SAR, China

Received November 21, 2003; E-mail: cmche@hku.hk

Abstract: The synthesis and structural, spectroscopic, and electrochemical properties of a series of trinuclear tridentate cyclometalated platinum(II) complexes tethered by bis(diphenylphosphinomethyl)phenylphosphine (dpmp) have been studied and compared with their mono- and binuclear homologues and a propeller-like congener. The X-ray crystal structures of several derivatives show the presence of a variety of intramolecular Pt···Pt, $\pi-\pi$, and C−H···O(crown ether) and intermolecular $\pi-\pi$ interactions. The trinuclear complexes display strong absorption in the 400−600 nm region and show intense red to near-infrared phosphorescence with microsecond lifetimes in fluid and glassy solutions and in the solid state. These emissions are generally assigned as ^{3}MMLCT [d$\sigma^*\rightarrow\pi^*$(C^N^N)] in nature. The close similarities between the emission energies in acetonitrile solution and in the solid state at 298 K indicate that comparable Pt···Pt and $\pi-\pi$ configurations are maintained in both media, and hence a relationship between the photophysical behavior of these lumophores and their solid-state structural features is proposed. The tendencies of the absorption and emission energies to red-shift from mono- to linearly tethered bi- and trinuclear Pt(II) species are evident. A light-emitting electrochemical cell using a trinuclear Pt(II) derivative as emitter has been demonstrated.

Introduction

One of the most exciting applications of transition metal complexes is the development of organometallic-based optoelectronics, such as light-emitting devices, chemosensors, and photovoltaic dye-sensitized devices.[1] For these purposes, cyclometalating and/or oligopyridine complexes of Ru(II),[2] Os(II),[3] Re(I),[4] and Ir(III),[5] which all have a d^6 electronic configuration, have been extensively studied for their long triplet excited-state lifetimes, high emission quantum yields, and tunable excited-state properties. Pt(II) complexes with cyclometalating or oligopyridine ligands, which exhibit a square-planar d^8 electronic configuration, have also been demonstrated

(1) (a) Balzani, V.; Credi, A.; Scandola, F. In *Transition Metals in Supramolecular Chemistry*; Fabbrizzi, L., Poggi, A., Eds.; Kluwer: Dordrecht, The Netherlands, 1994. (b) Lehn, J. M. *Supramolecular Chemistry-Concepts and Perspectives*; VCH: Weinheim, Germany, 1995. (c) Bignozzi, C. A.; Schoonover, J. R.; Scandola, F. *Prog. Inorg. Chem.* **1997**, *44*, 1−95.

(2) (a) Gao, F. G.; Bard, A. J. *J. Am. Chem. Soc.* **2000**, *122*, 7426−7427. (b) Grätzel, M. *Nature* **2001**, *414*, 338−344. (c) Osawa, M.; Hoshino, M.; Wakatsuki, Y. *Angew. Chem., Int. Ed.* **2001**, *40*, 3472−3474. (d) Anzenbacher, P., Jr.; Tyson, D. S.; Jursikova, K.; Castellano, F. N. *J. Am. Chem. Soc.* **2002**, *124*, 6232−6233. (e) Glazer, E. C.; Tor, Y. *Angew. Chem., Int. Ed.* **2002**, *41*, 4022−4026. (f) Galoppini, E.; Guo, W.; Zhang, W.; Hoertz, P. G.; Qu, P.; Meyer, G. J. *J. Am. Chem. Soc.* **2002**, *124*, 7801−7811. (g) Welter, S.; Brunner, K.; Hofstraat, J. W.; De Cola, L. *Nature* **2003**, *421*, 54−57. (h) Passalacqua, R.; Loiseau, F.; Campagna, S.; Fang, Y. Q.; Hanan, G. S. *Angew. Chem., Int. Ed.* **2003**, *42*, 1608−1611. (i) Chow, C. F.; Chiu, B. K. W.; Lam, M. H. W.; Wong, W. Y. *J. Am. Chem. Soc.* **2003**, *125*, 7802−7803.

(3) (a) Cameron, C. G.; Pickup, P. G. *J. Am. Chem. Soc.* **1999**, *121*, 7710−7711. (b) Breu, J.; Kratzer, C.; Yersin, H. *J. Am. Chem. Soc.* **2000**, *122*, 2548−2555. (c) Carlson, B.; Phelan, G. D.; Kaminsky, W.; Dalton, L.; Jiang, X.; Liu, S.; Jen, A. K. Y. *J. Am. Chem. Soc.* **2002**, *124*, 14162−14172.

(4) (a) Sun, S. S.; Lees, A. J. *Chem. Commun.* **2000**, 1687−1688. (b) Lo, K. K. W.; Hui, W. K.; Ng, D. C. M. *J. Am. Chem. Soc.* **2002**, *124*, 9344−9345. (c) Yam, V. W. W. *Chem. Commun.* **2001**, 789−796.

(5) (a) Dixon, I. M.; Collin, J. P.; Sauvage, J. P.; Flamigni, L.; Encinas, S.; Barigelletti, F. *Chem. Soc. Rev.* **2000**, 385−391. (b) Lamansky, S.; Djurovich, P.; Murphy, D.; Abdel-Razzaq, F.; Lee, H. E.; Adachi, C.; Burrow, P. E.; Forrest, S. R.; Thompson, M. E. *J. Am. Chem. Soc.* **2001**, *123*, 4304−4312. (c) Lo, K. K. W.; Ng, D. C. M.; Chung, C. K. *Organometallics* **2001**, *20*, 4999−5001. (d) Nazeeruddin, Md. K.; Humphry-Baker, R.; Berner, D.; Rivier, S.; Zuppiroli, L.; Graetzel, M. *J. Am. Chem. Soc.* **2003**, *125*, 8790−8797. (e) Finkenzeller, W. J.; Yersin, H. *Chem. Phys. Lett.* **2003**, *377*, 299−305.

(6) (a) Gliemann, G.; Yersin, H. *Struct. Bonding* **1985**, *62*, 87−153. (b) Miskowski, V. M.; Houlding, V. H. *Inorg. Chem.* **1989**, *28*, 1529−1533. (c) Biedermann, J.; Gliemann, G.; Klement, U.; Range, K. J.; Zabel, M. *Inorg. Chem.* **1990**, *29*, 1884−1888. (d) Miskowski, V. M.; Houlding, V. H. *Inorg. Chem.* **1991**, *30*, 4446−4452. (e) Miskowski, V. M.; Houlding, V. H.; Che, C. M.; Wang, Y. *Inorg. Chem.* **1993**, *32*, 2518−2524. (f) Connick, W. B.; Miskowski, V. M.; Houlding, V. H.; Gray, H. B. *Inorg. Chem.* **2000**, *39*, 2585−2592.

(7) (a) Maestri, M.; Sandrini, D.; Balzani, V.; Chassot, L.; Jolliet, P.; von Zelewsky, A. *Chem. Phys. Lett.* **1985**, *122*, 375−379. (b) Chassot, L.; von Zelewsky, A.; Sandrini, D.; Maestri, M.; Balzani, V. *J. Am. Chem. Soc.* **1986**, *108*, 6084−6085. (c) Gianini, M.; Forster, A.; Haag, P.; von Zelewsky, A.; Stoeckli-Evans, H. *Inorg. Chem.* **1996**, *35*, 4889−4895. (d) Yersin, H.; Humbs, W. *Inorg. Chem.* **1999**, *38*, 5820−5831. (e) Shi, J. C.; Chao, H. Y.; Fu, W. F.; Peng, S. M.; Che, C. M. *J. Chem. Soc., Dalton Trans.* **2000**, 3128−3132. (f) Brooks, J.; Babayan, Y.; Lamansky, S.; Djurovich, P. I.; Tsyba, I.; Bau, R.; Thompson, M. E. *Inorg. Chem.* **2002**, *41*, 3055−3066. (g) Yersin, H.; Donges, D.; Humbs, W.; Strasser, J.; Sitters, R.; Glasbeek, M. *Inorg. Chem.* **2002**, *41*, 4915−4922.

(8) (a) Zuleta, J. A.; Chesta, C. A.; Eisenberg, R. *J. Am. Chem. Soc.* **1989**, *111*, 8916−8917. (b) Cummings, S. D.; Eisenberg, R. *J. Am. Chem. Soc.* **1996**, *118*, 1949−1960. (c) Huertas, S.; Hissler, M.; McGarrah, J. E.; Lachicotte, R. J.; Eisenberg, R. *Inorg. Chem.* **2001**, *40*, 1183−1188. (d) Hissler, M.; Connick, W. B.; Geiger, D. K.; McGarrah, J. E.; Lipa, D.; Lachicotte, R. J.; Eisenberg, R. *Inorg. Chem.* **2000**, *39*, 447−457.

to be strongly emissive in fluid solution and the solid state, and have recently received considerable attention in material science.[6−11] The open square-planar geometry of Pt(II) allows axial substrate-binding, and this results in different photophysical and -chemical properties when compared to d^6 octahedral metal lumophores which display sphere-like coordination environments. Diverse excited states that emit in the visible spectral range have been reported for this class of complexes, and these include metal-centered ^{3}(dd), ligand-centered $^3(\pi\pi^*)$, excimeric $^3(\pi\pi^*)$, metal-to-ligand charge-transfer ^{3}MLCT, and metal−metal-to-ligand charge-transfer ^{3}MMLCT (or $[d\sigma^*\rightarrow\pi^*]$). Pt(II) complexes displaying emission in the yellow to red region or showing intense absorption in the near-infrared region have found applications in high-performance organic light-emitting[12] and photovoltaic dye-sensitized[13] devices. Furthermore, there have been active studies in developing emissive Pt(II) complexes as luminescent probes for biomolecular targets such as DNA and proteins.[14] Very recently, the realization of supramolecular recognition derived from Pt···Pt interactions in a predesigned metal-based molecular receptor was described by Bosnich and co-workers.[15]

The $[(C\hat{}N\hat{}N)Pt]^+$ moiety (HC^N^N = 6-aryl-2,2′-bipyridine) and its derivatives[11] were chosen in this study as the building unit for assembly of oligonuclear Pt(II) complexes due to their rich photoluminescent properties in fluid solutions. With regards to the terpyridine[9] and C^N^C (HC^N^CH = 2,6-diphenylpyridine)[10] complexes, the C^N^N ligand is a superior σ-donor than terpyridine but a more capable π-acceptor than C^N^C. Hence, the unique nature of the C^N^N auxiliary apparently affords ^{3}(dd) excited states (responsible for deactivation of Pt(II) photoluminescence) that are higher in energy relative to the ^{3}MLCT and/or $^3(\pi\pi^*)$ states. However, strong visible absorptions and near-infrared (NIR) emissions in fluid solutions are difficult to attain in monomeric $[(C\hat{}N\hat{}N)PtL]^{n+}$ (L = halide, acetylide, phosphine, pyridine, etc.; n = 0, 1) complexes, which typically show absorption and emission bands that are higher in energy compared to the well-studied $[Ru(\text{aromatic }\alpha\text{-diimine})_3]^{2+}$ system. This clearly hinders the utilization of cyclometalated Pt(II) complexes as photocatalysts for solar-energy conversion and as luminescent probes in biomedical applications. We envisioned that it would be feasible for the absorption and emission energies of this class of lumophores to be red-shifted through $d^8\cdots d^8$ and/or ligand−ligand interactions between $[(C\hat{}N\hat{}N)Pt]^+$ moieties.[16] The aim of the present study is to illustrate the intriguing structural and spectroscopic properties of multinuclear cyclometalated Pt(II) complexes that are tethered in linear or propeller conformations by oligophosphine ligands. Furthermore, the perturbation of low-energy emissions by weak noncovalent interactions, such as $d^8\cdots d^8$ (Pt···Pt), $\pi-\pi$, and C−H···O, will be highlighted.

Results

Synthesis. The tridentate cyclometalating ligands used in this study contain the 2,2′-bipyridine moiety plus a 6-aryl group which acts as a proton-donor to facilitate the cyclometalating process. Depending on the pendant functional groups, these ligands can be synthesized by various routes (see Scheme S1 in Supporting Information). 4,4′-Bis(*tert*-butyl)-6-phenyl-2,2′-bipyridine was prepared by reaction of phenyllithium and 4,4′-bis(*tert*-butyl)-2,2′-bipyridine, a method adopted by Hamilton and co-workers in the synthesis of 2-phenyl-1,10-phenanthroline.[17] 4-Hydroxycarbonyl-6-phenyl-2,2′-bipyridine and 6-(2-thienyl)-2,2′-bipyridine were obtained by condensation between acalkylpyridinium salts and α,β-unsaturated ketones in the presence of ammonium acetate in methanol.[18] Compounds **3**[19] and **4** are useful precursors to 4-substituted (HC^N^N) ligands, because the ^{n}Bu$_3$Sn and iodo groups can be readily substituted through established palladium(II)/copper(I)-catalyzed cross-coupling and amination protocols.[20] Heating a mixture of **4** and aza-15-crown-5 gave **5** bearing a crown ether moiety. This method was previously employed by Ward and co-workers to prepare 4-(aza-18-crown-6)-2,2′:6′,2″-terpyridine.[21] Refluxing these ligands with K_2PtCl_4 in CH_3CN/H_2O or with $PtCl_2$ in $C_2H_5OC_2H_4OH/H_2O$ gave the desired Cl-ligated precursors. The tridentate ligand bis(diphenylphosphinomethyl)phenylphosphine (dpmp) was synthesized according to the literature method.[22]

(9) (a) Bailey, J. A.; Hill, M. G.; Marsh, R. E.; Miskowski, V. M.; Schaefer, W. P.; Gray, H. B. *Inorg. Chem.* **1995**, *34*, 4591−4599. (b) Arena, G.; Calogero, G.; Campagna, S.; Monsu Scolaro, L.; Ricevuto, V.; Romeo, R. *Inorg. Chem.* **1998**, *37*, 2763−2769. (c) Lai, S. W.; Chan, M. C. W.; Cheung, K. K.; Che, C. M. *Inorg. Chem.* **1999**, *38*, 4262−4267. (d) Michalec, J. F.; Bejune, S. A.; McMillin, D. R. *Inorg. Chem.* **2000**, *39*, 2708−2709. (e) Yam, V. W. W.; Tang, R. P. L.; Wong, K. M. C.; Ko, C. C.; Cheung, K. K. *Inorg. Chem.* **2001**, *40*, 571−574. (f) Yam, V. W. W.; Wong, K. M. C.; Zhu, N. *J. Am. Chem. Soc.* **2002**, *124*, 6506−6507.

(10) (a) Lu, W.; Chan, M. C. W.; Cheung, K. K.; Che, C. M. *Organometallics* **2001**, *20*, 2477−2486. (b) Yam, V. W. W.; Tang, R. P. L.; Wong, K. M. C.; Lu, X. X.; Cheung, K. K.; Zhu, N. *Chem.-Eur. J.* **2002**, *8*, 4066−4076.

(11) (a) Chan, C. W.; Lai, T. F.; Che, C. M.; Peng, S. M. *J. Am. Chem. Soc.* **1993**, *115*, 11245−11253. (b) Cheung, T. C.; Cheung, K. K.; Peng, S. M.; Che, C. M. *J. Chem. Soc., Dalton Trans.* **1996**, 1645−1651. (c) Neve, F.; Ghedini M.; Crispini, A. *J. Chem. Soc., Chem. Commun.* **1996**, 2463−2464. (d) Neve, F.; Crispini, A.; Campagna, S. *Inorg. Chem.* **1997**, *36*, 6150−6156. (e) Lai, S. W.; Chan, M. C. W.; Cheung, T. C.; Peng, S. M.; Che, C. M. *Inorg. Chem.* **1999**, *38*, 4046−4055. (f) Lai, S. W.; Chan, M. C. W.; Cheung, K. K.; Che, C. M. *Organometallics* **1999**, *18*, 3327−3336. (g) Yip, J. H. K.; Suwarno; Vittal, J. J. *Inorg. Chem.* **2000**, *39*, 3537−3543. (h) Che, C. M.; Fu, W. F.; Lai, S. W.; Hou, Y. J.; Liu, Y. L. *Chem. Commun.* **2003**, 118−119.

(12) (a) Chan, S. C.; Chan, M. C. W.; Wang, Y.; Che, C. M.; Cheung, K. K.; Zhu, N. *Chem.-Eur. J.* **2001**, *7*, 4180−4190. (b) Lu, W.; Mi, B. X.; Chan, M. C. W.; Hui, Z.; Zhu, N.; Lee, S. T.; Che, C. M. *Chem. Commun.* **2002**, 206−207. (c) Adamovich, V.; Brooks, J.; Tamayo, A.; Alexander, A. M.; Djurovich, P. I.; D'Andrade, B. W.; Adachi, C.; Forrest, S. R.; Thompson, M. E. *New J. Chem.* **2002**, *26*, 1171−1178. (d) D'Andrade, B. W.; Brooks, J.; Adamovich, V.; Thompson, M. E.; Forrest, S. R. *Adv. Mater.* **2002**, *14*, 1032−1036. (e) Lin, Y. Y.; Chan, S. C.; Chan, M. C. W.; Hou, Y. J.; Zhu, N.; Che, C. M.; Liu, Y.; Wang, Y. *Chem.-Eur. J.* **2003**, *9*, 1263−1272. (f) Lu, W.; Mi, B. X.; Chan, M. C. W.; Hui, Z.; Che, C. M.; Zhu, N.; Lee, S. T. *J. Am. Chem. Soc.* **2004**, *126*, 4958−4971.

(13) (a) Islam, A.; Sugihara, H.; Hara, K.; Singh, L. P.; Katoh, R.; Yanagida, M.; Takahashi, Y.; Murata, S.; Arakawa, H.; Fujihashi, G. *Inorg. Chem.* **2001**, *40*, 5371−5380. (b) McGarrah, J. E.; Kim, Y. J.; Hissler, M.; Eisenberg, R. *Inorg. Chem.* **2001**, *40*, 4510−4511. (c) McGarrah, J. E.; Eisenberg, R. *Inorg. Chem.* **2003**, *42*, 4355−4365.

(14) (a) Barton, J. K.; Lippard, S. J. *Biochemistry* **1979**, *18*, 2661−2668. (b) Liu, H. Q.; Cheung, T. C.; Che, C. M. *Chem. Commun.* **1996**, 1039−1040. (c) Che, C. M.; Yang, M.; Wong, K. H.; Chan, H. L.; Lam, W. *Chem.-Eur. J.* **1999**, *5*, 3350−3356. (d) Che, C. M.; Zhang, J. L.; Lin, L. R. *Chem. Commun.* **2002**, 2556−2557. (e) Ma, D. L.; Che, C. M. *Chem.-Eur. J.* **2003**, *9*, 6133−6144.

(15) (a) Goshe, A. J.; Steele, I. M.; Bosnich, B. *J. Am. Chem. Soc.* **2003**, *125*, 444−451. (b) Goshe, A. J.; Steele, I. M.; Ceccarelli, C.; Rheingold, A. L.; Bosnich, B. *Proc. Natl. Acad. Sci. U.S.A.* **2002**, *99*, 4823−4829. (c) Sommer, R. D.; Rheingold, A. L.; Goshe, A. J.; Bosnich, B. *J. Am. Chem. Soc.* **2001**, *123*, 3940−3952.

(16) Lu, W.; Zhu, N.; Che, C. M. *Chem. Commun.* **2002**, 900−901.

(17) Goodman, M. S.; Hamilton, A. D.; Weiss, J. *J. Am. Chem. Soc.* **1995**, *117*, 8447−8455.

(18) Kröhnke, F. *Synthesis* **1976**, 1−24.

(19) (a) Pabst, G. R.; Pfüller, O. C.; Sauer, J. *Tetrahedron* **1999**, *55*, 5047−5066. (b) Pabst, G. R.; Sauer, J. *Tetrahedron* **1999**, *55*, 5067−5088. (c) Sauer, J.; Heldmann, D. K.; Pabst, G. R. *Eur. J. Org. Chem.* **1999**, 313−321.

(20) (a) *Cross-Coupling Reactions: A Practical Guide*; Miyaura, N., Ed.; Springer: Berlin, Germany, 2002. (b) Ley, S. V.; Thomas, A. W. *Angew. Chem., Int. Ed.* **2003**, *42*, 5400−5449.

(21) Whittle, B.; Batten, S. R.; Jeffery, J. C.; Rees, L. H.; Ward, M. D. *J. Chem. Soc., Dalton Trans.* **1996**, 4249−4255.

(22) Appel, R.; Geisler, K.; Schöler, H. F. *Chem. Ber.* **1979**, *112*, 648−653.

Chart 1

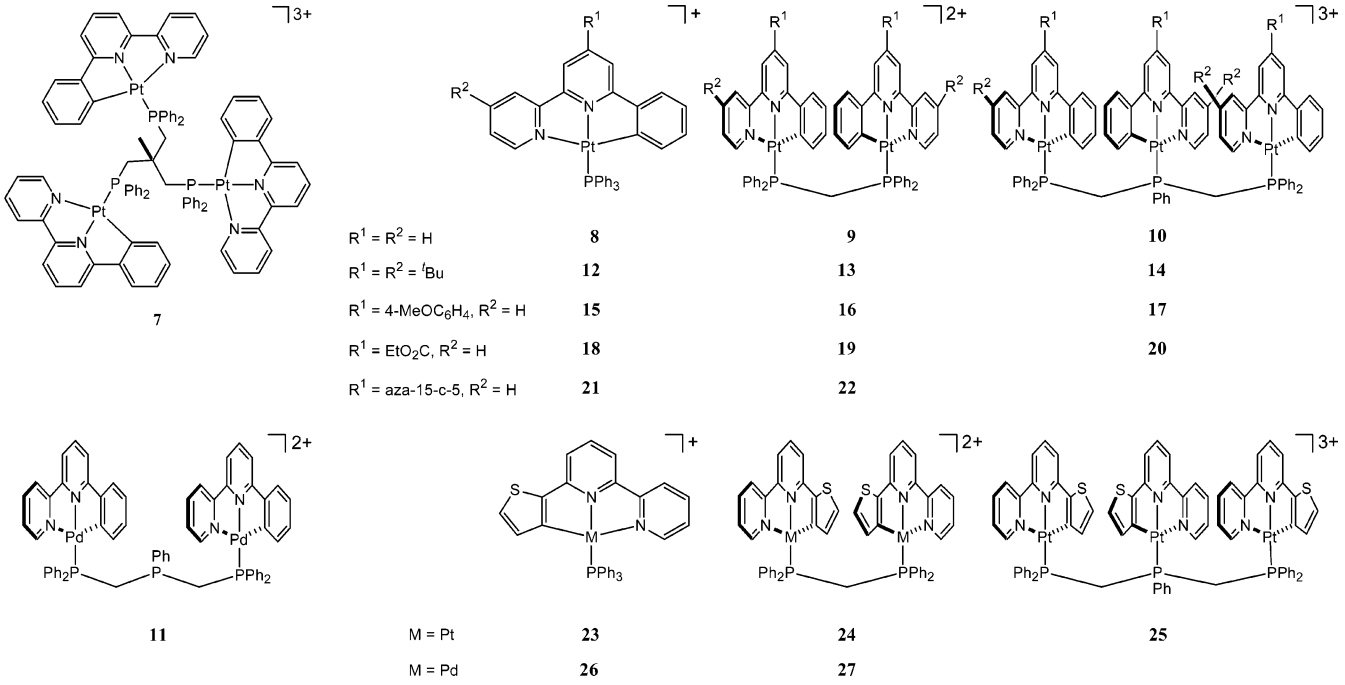

The trinuclear $[\{R^x(C\text{^}N\text{^}N)\}_3Pt_3(\mu_3\text{-triphosphine})]^{3+}$ (R^x denotes substituent(s) on (C^N^N), Chart 1) derivatives were prepared by reacting $[R^x(C\text{^}N\text{^}N)PtCl]$ with the triphosphine ligands 1,1,1-tris(diphenylphosphinomethyl)ethane (tppe) and dpmp in a CH_2Cl_2/CH_3OH mixture followed by counterion metathesis. For comparison, their mono- and binuclear homologues with triphenylphosphine (PPh_3) and bis(diphenylphosphino)methane (dppm) ligands, respectively, have also been prepared. Several attempts to synthesize the Pd_3 counterparts were undertaken but have not been successful; treatment of three molar equivalents of [(C^N^N)PdCl] with dpmp resulted in the isolation of the binuclear complex $[(C\text{^}N\text{^}N)_2Pd_2(\mu\text{-dpmp})]^{2+}$ (**11**), which has been characterized by ^1H (only one set of signals for (C^N^N) ligands) and ^{31}P (one signal for bound P and one for free P [lower intensity]) NMR spectroscopy to contain tethered [(C^N^N)Pd] moieties on the two terminal phosphorus atoms with a free central phosphorus atom.

The ^{31}P NMR spectrum of **10**$(ClO_4)_3$ contains only one signal (with ^{195}Pt satellites: $^1J_{P-Pt} = 4070$ Hz) at 26 °C in CD_3CN, but there are clearly at least two types of phosphorus nuclei in different chemical environments in this molecule. Subsequent variable-temperature ^{31}P NMR measurements for **10**$(ClO_4)_3$ in CD_3COCD_3/CD_3CN (1/1, v/v) revealed two groups of signals (see Supporting Information for spectra). Upon decreasing the temperature from +60 to −60 °C, the chemical shift for the central P atom experiences a downfield shift from 11.3 to 13.7 ppm, while that for the peripheral P atoms (higher intensity) shifts upfield from 12.6 to 11.7 ppm. No fluxional behavior was detected for **10**$(ClO_4)_3$; thus, it appears that the central $[(C\text{^}N\text{^}N)Pt]^+$ unit "swings" between the two terminal $[(C\text{^}N\text{^}N)Pt]^+$ moieties at a sufficiently fast rate so that the environments of the latter average out (or remain the same) even down to −60 °C.

The $^{195}Pt[^{31}P]$ NMR spectrum of **10**$(ClO_4)_3$ shows two doublets at −3847 (central) and −3976 (terminal) ppm ($^1J_{P-Pt} = 4091$ and 4114 Hz, respectively). A downfield shift for the ^{195}Pt signals from mono- to bi- and trinuclear species in the present study is evident; hence, the ^{195}Pt NMR signals appear at −4160, −4008, and −3843/−3969 (central/terminal) ppm for **12**(ClO_4), **13**$(ClO_4)_2$, and **14**$(ClO_4)_3$ in the [4,4′-^{t}Bu$_2$(C^N^N)Pt] series, −4157, −3982, and −3820/−3962 ppm for **18**(ClO_4), **19**$(ClO_4)_2$, and **20**$(ClO_4)_3$ in the [4-EtO$_2$C-(C^N^N)Pt] series, and −4240, −4092, and −3941/−4061 ppm for **23**(ClO_4), **24**$(ClO_4)_2$, and **25**$(ClO_4)_3$ in the [(S^N^N)Pt] series, respectively. It is interesting to note that for each higher homologue in the series, the corresponding ^{195}Pt NMR signal systematically shifts downfield by 160 ± 10 ppm. This trend to shift downfield for the ^{195}Pt NMR signals is consistent with that observed by Bosnich and co-workers in their studies on the "supramolecular" recognition and formation of metal-based host−guest complexes through Pt···Pt/ligand−ligand interactions.[15a]

Solid-State Pt···Pt and $\pi-\pi$ Interactions. The crystal structures of **7**$(ClO_4)_3$, **10**$(ClO_4)_3\cdot H_2O$, **10**$(ClO_4)_3\cdot 2Et_2O\cdot CH_3CN$, and **25**$(ClO_4)_3\cdot 1.5Et_2O\cdot CH_3CN$ were reported in our previous communication,[16] and the remaining crystal data are listed in the Supporting Information. The structure of **7**$(ClO_4)_3$ shows three $[(C\text{^}N\text{^}N)Pt]^+$ units arranged in C_{3v} symmetry through coordination of the P donors of the tripodal tppe ligand to Pt(II). In contrast, the dpmp ligand can position multiple $[(C\text{^}N\text{^}N)Pt]^+$ moieties into linear face-to-face configurations. Upon diffusion of diethyl ether vapor into an acetonitrile solution of **10**$(ClO_4)_3$, three crystal forms of yellow, orange, and red coloration were obtained. For **10**$(ClO_4)_3\cdot H_2O$ (red form), the intramolecular metal···metal contacts of 3.194 Å at Pt1···Pt2 and 3.399 Å at Pt2···Pt3, with the Pt1···Pt2···Pt3 angle being 169°, indicate weak $d^8\cdots d^8$ interactions across Pt1···Pt2···Pt3. The yellow and orange forms quickly transform into the red form upon removal from the mother liquor. Nevertheless, the molecular structure of the orange form (**10**$(ClO_4)_3\cdot 2Et_2O\cdot CH_3CN$) was determined by X-ray crystallography. The intramolecular metal···metal contacts are 3.364 Å (Pt1···Pt2) and 3.617

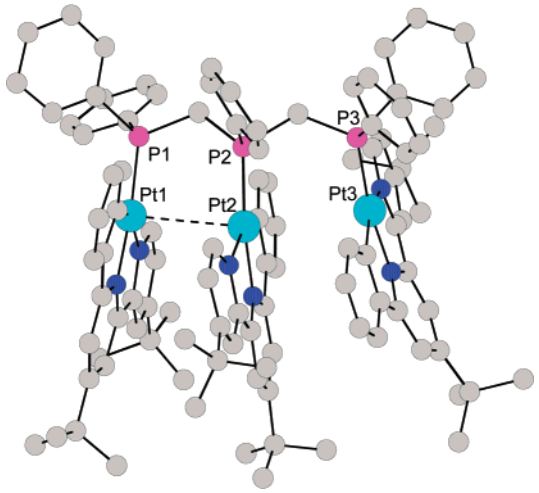

Figure 1. Perspective view of the cation of **14**$(ClO_4)_3$·$3CH_3CN$.

Å (Pt2···Pt3), and the Pt1···Pt2···Pt3 angle is 162°. Hence, a weak d^8···d^8 interaction exists between Pt1···Pt2, but the value of the Pt2···Pt3 separation (3.617 Å) is beyond the range of intermetal distances (3.09−3.50 Å) normally observed in monomeric Pt(II) extended linear-chain structures.[6d] In addition, it is apparent that two neighboring cations of **10** in the orange form are engaged in intermolecular $\pi-\pi$ interactions (ca. 3.5 Å between $[(C\hat{}N\hat{}N)Pt]^+$ planes at Pt3). Furthermore, the color of crystalline complex **10** depends on the counterions. For **10**$(BF_4)_3$, only the orange form was found in the mother liquor, and this slowly transformed into the red form upon collection on a sinter-glass filter. For **10**$(PF_6)_3$, only the red form was observed in the mother liquor or under reduced pressure. After prolonged standing, all orange/red forms of these solids slowly turn brownish red in color, presumably due to lattice contraction induced by loss of solvated molecules.

For complex **14**, two *tert*-butyl groups are introduced at each (C^N^N) ligand to increase the steric repulsion between neighboring [(C^N^N)Pt] moieties. A perspective view of the complex cation of **14**$(ClO_4)_3$·$3CH_3CN$ is shown in Figure 1. The three $[4,4'\text{-}{}^t\text{Bu}_2(C\hat{}N\hat{}N)Pt]^+$ fragments are partially staggered, with torsion angles of 29.6° and 9.3° about the Pt1−Pt2 and Pt2−Pt3 axes, respectively (defined by the angle between the Pt1−Pt2−N2 and Pt1−Pt2−N4 planes and that between the Pt2−Pt3−N2 and Pt2−Pt3−N6 planes, respectively). The intramolecular metal···metal contacts are 3.217 Å at Pt1···Pt2 and 3.601 Å at Pt2···Pt3, and the Pt1···Pt2···Pt3 angle is 157°, resembling those values for the orange form of **10**. Similarly, we propose that the weak d^8···d^8 interaction is present between Pt1···Pt2 but not Pt2···Pt3. The salient difference between the crystal structure of **14**$(ClO_4)_3$·$3CH_3CN$ and **10**$(ClO_4)_3$·$2Et_2O$·CH_3CN (orange form) is that the latter undergoes dimeric $\pi-\pi$ interactions with an adjacent molecule, but the bulkiness of the $[4,4'\text{-}{}^t\text{Bu}_2(C\hat{}N\hat{}N)Pt]^+$ moieties presumably disfavors this.

A perspective view of the complex cation of **20**$(ClO_4)_3$·$2CH_3CN$ is shown in Figure 2 (top). The three $[4\text{-}EtO_2C(C\hat{}N\hat{}N)Pt]^+$ groups are staggered, with torsion angles of 33.7° about the Pt1−Pt2 axis and 8.9° about Pt2−Pt3, respectively. The intramolecular metal···metal contacts are 3.466 Å at Pt1···Pt2 and 3.647 Å at Pt2···Pt3, and the Pt1···Pt2···Pt3 angle is 162°; hence, Pt1···Pt2 but not Pt2···Pt3 appears to undergo a weak d^8···d^8 interaction. These structural data are similar to those for **10**$(ClO_4)_3$·$2Et_2O$·CH_3CN (orange form) and **14**$(ClO_4)_3$·$3CH_3CN$, but the crystal packing of **20**$(ClO_4)_3$·$2CH_3CN$ is different. The $[4\text{-}EtO_2C(C\hat{}N\hat{}N)Pt]^+$ moieties in **20**$(ClO_4)_3$·$2CH_3CN$ are arranged into infinite chains through intramolecular Pt···Pt and intermolecular $\pi-\pi$ interactions, as depicted in Figure 2 (bottom). The intermolecular $\pi-\pi$ stacking occurs between the $[4\text{-}EtO_2C(C\hat{}N\hat{}N)Pt]^+$ planes of Pt1 and Pt3, which contrasts with that in crystal **10**$(ClO_4)_3$·$2Et_2O$·CH_3CN where dimeric $\pi-\pi$ contacts occur between two $[(C\hat{}N\hat{}N)Pt]^+$ moieties at Pt3. As a consequence of the noncovalent interactions, the molecular cations are packed in a coiled/helical conformation, where one turn contains two cations and a screw-pitch of 20.8 Å is observed.

In the crystal structure of **6** (see Supporting Information for perspective view and packing diagram), the oxygen atoms on the crown ether moiety are not involved in intermolecular interactions. Neighboring (C^N^N) planes are stacked into dimeric structures in a head-to-tail manner through $\pi-\pi$ interaction. The interlayer distance is ca. 3.6 Å, but the shortest Pt···Pt distance is 6.609 Å.

Perspective views of the cation in crystal **22**$(PF_6)_2$ are shown in Figure 3. Unlike previous dppm-tethered [(C^N^N)Pt] complexes, the long Pt···Pt separation of 3.827 Å in **22**$(PF_6)_2$ is beyond the range expected for appreciable intermetal interaction. The two $[4\text{-(aza-15-crown-5)}(C\hat{}N\hat{}N)Pt]^+$ moieties are staggered with a torsion angle of 43.2° about the Pt···Pt axis. Close scrutiny of this structure reveals short contacts between H3 on the 4′-position of the diimine ligand and the oxygen atoms (O2−O4) on the crown ether pendant of the adjacent $[4\text{-(aza-15-crown-5)}(C\hat{}N\hat{}N)Pt]^+$ fragment, and vice versa (e.g. C3···O3 3.439 and H3···O3 2.598 Å). These oxygen atoms protrude toward the closest hydrogen atom, while the nitrogen atoms do not appear to be significantly involved in these weak hydrogen-bonding interactions.

Perspective views of cations in **24**$(ClO_4)_2$·$2CH_3CN$ and **25**$(ClO_4)_3$·$1.5Et_2O$·CH_3CN are shown in Figure 4. In the binuclear structure **24**, the two $[(S\hat{}N\hat{}N)Pt]^+$ fragments are staggered with a torsion angle of 29.0° about the Pt1−Pt2 axis. The intramolecular Pt···Pt distance is 3.321 Å. In the trinuclear structure **25**, the three $[(S\hat{}N\hat{}N)Pt]^+$ units are staggered with torsion angles of 33.0° about the Pt1−Pt2 axis and 18.7° about Pt2−Pt3, respectively. The intramolecular metal···metal separations are 3.254 Å at Pt1···Pt2 and 3.389 Å at Pt2···Pt3, and the Pt1···Pt2···Pt3 angle is 163°. Hence, weak d^8···d^8 interactions apparently exist between Pt1···Pt2 in **24** and across Pt1··· Pt2···Pt3 in **25**.

Electronic Spectroscopy. The UV−vis absorption data of the complexes in the present study are summarized in Table 1. A comparison between the electronic spectra of **7**$(ClO_4)_3$, **10**$(ClO_4)_3$, and **17**$(ClO_4)_3$ is shown in Figure 5. The UV−vis spectra of **10**$(ClO_4)_3$ and **17**$(ClO_4)_3$ in acetonitrile at 298 K feature broad absorptions in the 400−600 nm range with average ϵ values of ~5000 $dm^3\ mol^{-1}\ cm^{-1}$, which are almost double that (average $\epsilon \approx 2550\ dm^3\ mol^{-1}\ cm^{-1}$) previously found for the binuclear homologue $[(C\hat{}N\hat{}N)_2Pt_2(\mu\text{-dppm})](ClO_4)_2$ [**9**$(ClO_4)_2$]. The lowest-energy absorption peak maximum is located at 517 and 522 nm for **10**$(ClO_4)_3$ and **17**$(ClO_4)_3$, respectively. These transitions are not observed in the UV−vis spectra of the propeller-shaped **7**$(ClO_4)_3$ and the mono- [**8**(ClO_4) and **15**(ClO_4)] and binuclear [**9**$(ClO_4)_2$ and **16**$(ClO_4)_2$] relatives.

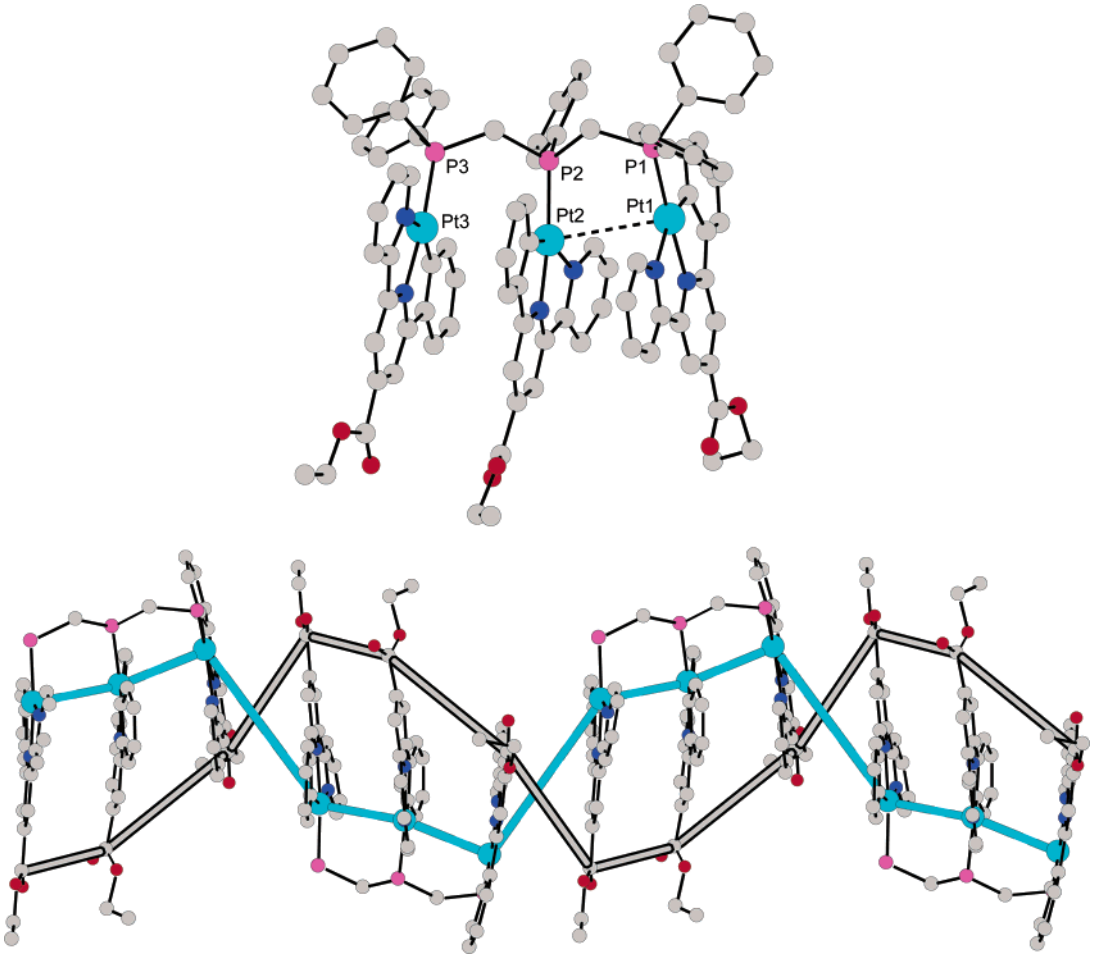

Figure 2. Top: perspective view of the cation of **20**$(ClO_4)_3$·$2CH_3CN$. Bottom: view of four neighboring cations of **20**$(ClO_4)_3$·$2CH_3CN$ (bold lines highlight the coiled nature of the structure; phenyl groups of dpmp ligands are omitted for clarity).

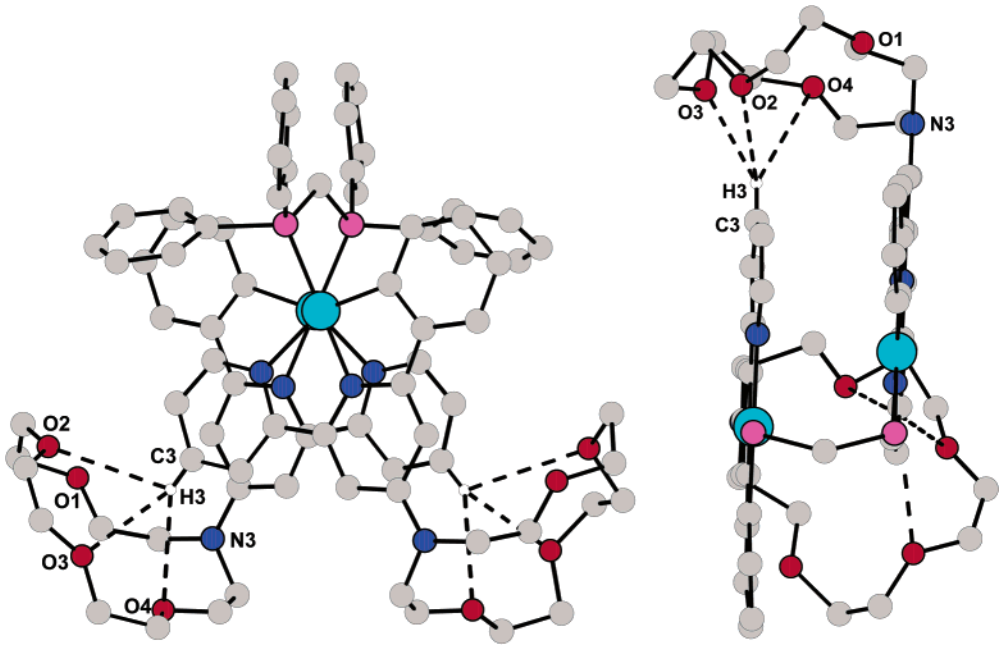

Figure 3. View along the Pt···Pt axial (left) and side view (right, phenyl groups of dppm ligand are omitted for clarity) of the cation of **22**$(PF_6)_2$ (C_2 axis exists for cation), with dashed lines indicating contacts shorter than the sum of van der Waals radii.

A comparison between the electronic spectra of **12**(ClO_4), **13**$(ClO_4)_2$, and **14**$(ClO_4)_3$ is shown in Figure 6. The UV−vis spectra of **13**$(ClO_4)_2$ and **14**$(ClO_4)_3$ in acetonitrile at 298 K feature broad absorptions in the 400−550 nm range, and the lowest-energy absorption peak maximum is ca. 500 nm for both **13**$(ClO_4)_2$ and **14**$(ClO_4)_3$. Clearly, such broad absorptions are

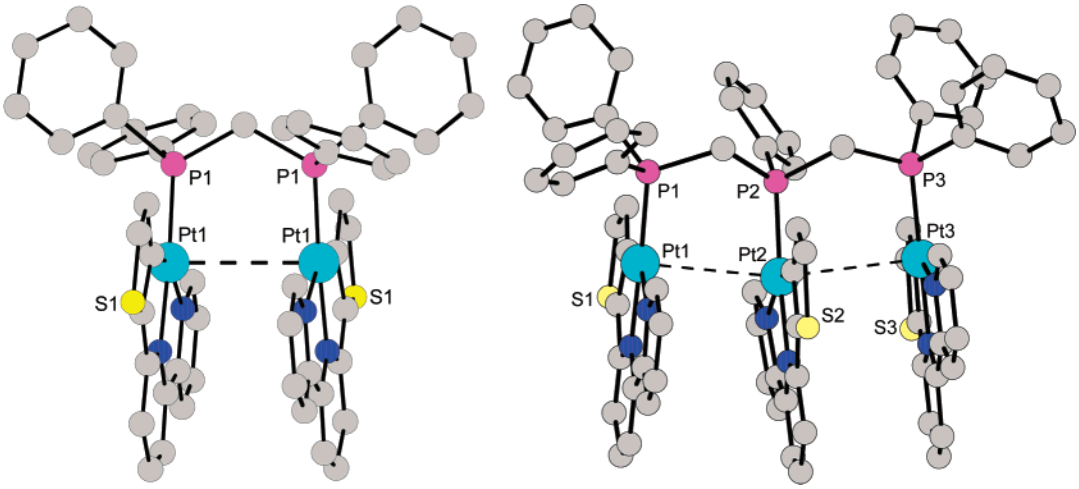

Figure 4. Perspective view of the cation of **24**$(ClO_4)_2$·2CH_3CN (left) and **25**$(ClO_4)_3$·1.5Et_2O·CH_3CN (right).

Table 1. Absorption Data[a]

complex	λ^{abs}/nm (ϵ/10^4 dm^3 mol^{-1} cm^{-1})
[(C^N^N)$_3$Pt$_3$(μ_3-tppe)](ClO_4)$_3$, **7**(ClO_4)$_3$	332 (3.17), 350 (2.95), 400 (sh, 0.14), 415 (sh, 0.12)
[(C^N^N)$_3$Pt$_3$(μ_3-dpmp)](ClO_4)$_3$, **10**(ClO_4)$_3$	337 (2.41), 424 (broad, 0.52), 482 (broad, 0.46), 513 (broad, 0.41)
[4,4′-^{t}Bu$_2$(C^N^N)PtPPh$_3$](ClO_4), **12**(ClO_4)	331 (1.24), 347 (1.18), 390 (broad sh, 0.05)
[{4,4′-^{t}Bu$_2$(C^N^N)}$_2$Pt$_2$(μ-dppm)](ClO_4)$_2$, **13**(ClO_4)$_2$	328 (1.41), 336 (1.40), 418 (broad, 0.44), 460 (broad sh, 0.31), 490 (broad sh, 0.18)
[{4,4′-^{t}Bu$_2$(C^N^N)}$_3$Pt$_3$(μ_3-dpmp)](ClO_4)$_3$, **14**(ClO_4)$_3$	in CH_3CN: 332 (2.56), 340 (sh, 2.47), 414 (broad, 0.56), 463 (broad sh, 0.41), 495 (0.25) in CH_2Cl_2: 336 (3.01), 346 (sh, 2.86), 417 (broad sh, 0.63), 463 (broad sh, 0.48), 495 (0.34) in C_2H_5OH: 332 (2.54), 340 (sh, 2.47), 417 (0.56), 462 (broad sh, 0.41), 491 (broad sh, 0.26) in C_6H_6: 336 (2.81), 344 (sh, 2.71), 424 (broad, 0.67), 464 (broad sh, 0.54), 493 (broad sh, 0.37)
[{4-(4-MeOC_6H_4)(C^N^N)}$_3$Pt$_3$(μ_3-dpmp)](ClO_4)$_3$, **17**(ClO_4)$_3$	344 (6.60), 420 (sh, 1.02), 494 (0.57), 522 (0.59)
[4-EtO$_2$C(C^N^N)PtPPh$_3$](ClO_4), **18**(ClO_4)	342 (1.47), 364 (1.08), 442 (broad sh, 0.04)
[{4-EtO$_2$C(C^N^N)}$_2$Pt$_2$(μ-dppm)](ClO_4)$_2$, **19**(ClO_4)$_2$	336 (1.51), 351 (1.54), 438 (0.35), 490 (broad sh, 0.22), 525 (broad sh, 0.16)
[{4-EtO$_2$C(C^N^N)}$_3$Pt$_3$(μ_3-dpmp)](ClO_4)$_3$, **20**(ClO_4)$_3$	342 (2.32), 356 (2.16), 441 (broad sh, 0.39), 492 (broad sh, 0.27), 539 (0.21)
[4-(aza-15-crown-5)(C^N^N)PtPPh$_3$](PF_6), **21**(PF_6)	317 (1.12), 321 (1.12), 374 (0.55)
[{4-(aza-15-crown-5)(C^N^N)}$_2$Pt$_2$(μ-dppm)](PF_6)$_2$, **22**(PF_6)$_2$	320 (1.69), 368 (0.93), 439 (broad sh, 0.28)
[(S^N^N)PtPPh$_3$]ClO_4, **23**(ClO_4)	342 (1.46), 460 (0.04)
[(S^N^N)$_2$Pt$_2$(μ-dppm)](ClO_4)$_2$, **24**(ClO_4)$_2$	345 (3.48), 437 (0.89), 495 (broad sh, 0.34)
[(S^N^N)$_3$Pt$_3$(μ_3-dpmp)](ClO_4)$_3$, **25**(ClO_4)$_3$	346 (2.79), 468 (0.85), 528 (broad sh, 0.41)
[(S^N^N)PdPPh$_3$]ClO_4, **26**(ClO_4)	311 (sh, 2.12), 319 (2.20), 421 (broad, 0.24)
[(S^N^N)$_2$Pd$_2$(μ-dppm)](ClO_4)$_2$, **27**(ClO_4)$_2$	312 (sh, 3.23), 425 (broad sh, 0.39)

[a] Recorded in CH_3CN solution at 298 K unless stated otherwise.

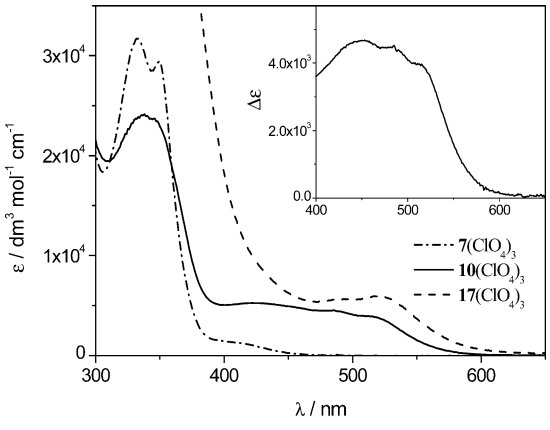

Figure 5. UV−vis absorption spectra of **7**$(ClO_4)_3$, **10**$(ClO_4)_3$, and **17**$(ClO_4)_3$ in acetonitrile at 298 K. Inset: Plot of $\Delta\epsilon$ versus wavelength for **7**$(ClO_4)_3$ and **10**$(ClO_4)_3$ in acetonitrile at 298 K.

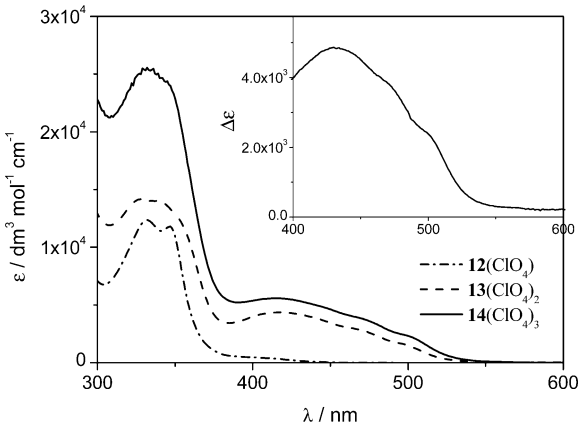

Figure 6. UV−vis absorption spectra of **12**(ClO_4), **13**$(ClO_4)_2$, and **14**$(ClO_4)_3$ in acetonitrile at 298 K. Inset: Plot of $\Delta\epsilon$ versus wavelength for **12**(ClO_4) (ϵ values multiplied by 3) and **14**$(ClO_4)_3$ in acetonitrile at 298 K.

not observed beyond 400 nm in the spectrum of the mononuclear species **12**(ClO_4).

Comparisons between the electronic spectra of **18**(ClO_4), **19**$(ClO_4)_2$, and **20**$(ClO_4)_3$ and between **23**(ClO_4), **24**$(ClO_4)_2$, and

Table 2. Emission Data

complex	solution,[a] 298 K λ_{max}/nm (τ/μs; ϕ[b])	glassy solution,[c] 77 K λ_{max}/nm (τ/μs)	solid state, 298 K λ_{max}/nm (τ/μs)	solid state, 77 K λ_{max}/nm (τ/μs)
[(C^N^N)$_3$Pt$_3$(μ_3-tppe)](ClO$_4$)$_3$, **7**(ClO$_4$)$_3$	520 (8.0; 0.12)	500 (16.0), 535	544 (5.9)	533 (9.6), 571
[(C^N^N)$_3$Pt$_3$(μ_3-dpmp)](ClO$_4$)$_3$, **10**(ClO$_4$)$_3$	710 (0.1; 0.02)	516 (16.7), 552; 677 (4.0)	orange form: 630 (1.5) red form: 674 (0.9) brown form: 709 (0.4)	red form: 680 (3.4) brown form: 730 (2.3)
[4,4′-^{t}Bu$_2$(C^N^N)PtPPh$_3$](ClO$_4$), **12**(ClO$_4$)	532 (1.0; 0.11)	488 (23.5), 524	532 (3.5)	516 (4.2), 548
[{4,4′-^{t}Bu$_2$(C^N^N)}$_2$Pt$_2$(μ-dppm)](ClO$_4$)$_2$, **13**(ClO$_4$)$_2$	625 (0.5; 0.05)	493, 530, 598 (6.5)	593 (2.0)	592 (3.5)
[{4,4′-^{t}Bu$_2$(C^N^N)}$_3$Pt$_3$(μ_3-dpmp)](ClO$_4$)$_3$, **14**(ClO$_4$)$_3$	in CH$_3$CN: 628 (1.7; 0.08) in C$_6$H$_6$: 621 (2.7; 0.18) in CH$_2$Cl$_2$: 631 (2.3; 0.15) in C$_2$H$_5$OH: 649 (0.6; 0.05)	501, 538, 607 (7.1)	617 (2.1)	619 (3.9)
[{4-(4-MeOC$_6$H$_4$)(C^N^N)}$_3$Pt$_3$(μ_3-dpmp)](ClO$_4$)$_3$, **17**(ClO$_4$)$_3$	710 (1.0; 0.05)	697 (3.6)	710 (1.1)	677 (1.6)
[4-EtO$_2$C(C^N^N)PtPPh$_3$](ClO$_4$), **18**(ClO$_4$)	562 (0.1; 0.01)	527 (20.0), 560	628 (3.5)	612 (5.2)
[{4-EtO$_2$C(C^N^N)}$_2$Pt$_2$(μ-dppm)](ClO$_4$)$_2$, **19**(ClO$_4$)$_2$	nonemissive	550 (10.7), 662 (6.2)	662 (1.8)	664 (3.9)
[{4-EtO$_2$C(C^N^N)}$_3$Pt$_3$(μ_3-dpmp)](ClO$_4$)$_3$, **20**(ClO$_4$)$_3$	nonemissive	562, broad	648 (0.9)	645 (3.4)
[4-(aza-15-crown-5)(C^N^N)PtPPh$_3$](PF$_6$), **21**(PF$_6$)	530 (2.3; 0.09)	n.d.	530 (2.7)	n.d.
[{4-(aza-15-crown-5)(C^N^N)}$_2$Pt$_2$(μ-dppm)](PF$_6$)$_2$, **22**(PF$_6$)$_2$	589 (0.7; 0.07)	475, 587 (4.7)	570 (0.4)	517, 578 (2.2)
[(S^N^N)PtPPh$_3$]ClO$_4$, **23**(ClO$_4$)	603 (4.7; 0.05)	613 (21.4), 665	627 (7.7)	642 (1.2)
[(S^N^N)$_2$Pt$_2$(μ-dppm)](ClO$_4$)$_2$, **24**(ClO$_4$)$_2$	629 (3.1; 0.02)	710 ($\leq$0.1), broad	723 ($\leq$0.1)	685 (0.5)
[(S^N^N)$_3$Pt$_3$(μ_3-dpmp)](ClO$_4$)$_3$, **25**(ClO$_4$)$_3$	657 (1.3; 0.01), broad	627 (1.0)	658 (0.4)	649 (1.3)
[(S^N^N)PdPPh$_3$]ClO$_4$, **26**(ClO$_4$)	nonemissive	547 (471), 592	nonemissive	nonemissive
[(S^N^N)$_2$Pd$_2$(μ-dppm)](ClO$_4$)$_2$, **27**(ClO$_4$)$_2$	nonemissive	558 (217), 602	nonemissive	nonemissive

[a] Measured in CH$_3$CN solution unless stated otherwise. [b] [Ru(bpy)$_3$](ClO$_4$)$_2$ in CH$_3$CN (ϕ = 0.062) as reference. [c] Measured in MeOH/EtOH (1/4, v/v), complex concentration $\sim 1 \times 10^{-5}$ mol dm^{-3}. n.d. = not determined.

25(ClO$_4$)$_3$ are shown in the Supporting Information. The UV−vis spectra for the bi- and trinuclear complexes in acetonitrile at 298 K feature broad absorptions in the 400−550 nm range, and the lowest-energy absorption peak maximum appears at ca. 529, 543, 437, and 468 nm for **19**(ClO$_4$)$_2$, **20**(ClO$_4$)$_3$, **24**(ClO$_4$)$_2$, and **25**(ClO$_4$)$_3$, respectively. Such broad bands beyond 400 nm are not observed in the spectra of the mononuclear homologues **18**(ClO$_4$) and **23**(ClO$_4$).

The UV−vis absorption spectra of **21**(PF$_6$) and **22**(PF$_6$)$_2$ in acetonitrile are shown in Figure 7. The salient difference between these two spectra occurs in the low-energy region; a broad band in the 425−500 nm range for the binuclear complex **22**(PF$_6$)$_2$ is absent for the monomeric species **21**(PF$_6$).

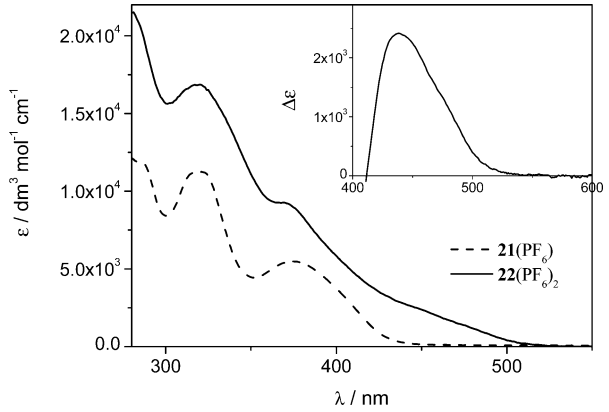

Figure 7. UV−vis absorption spectra of **21**(PF$_6$) and **22**(PF$_6$)$_2$ in acetonitrile at 298 K. Inset: Plot of $\Delta\epsilon$ versus wavelength for **21**(PF$_6$) (ϵ values multiplied by 2) and **22**(PF$_6$)$_2$ in acetonitrile at 298 K.

Steady-State Emission Spectra. The emission data of the complexes in the present study are summarized in Table 2. All Pt(II) complexes are emissive in the solid state, and in glassy and fluid solutions except for **19**(ClO$_4$)$_2$ and **20**(ClO$_4$)$_3$, which are virtually nonemissive in CH$_3$CN solution at 298 K. The observed emission lifetimes (in the microsecond range) and quantum yields in fluid solutions are comparable or superior to the widely studied [Ru(bpy)$_3$]$^{2+}$ complex.

The green-yellow solid-state emission (Figure 8, λ_{max} 544 nm) of the propeller-shaped derivative **7**(ClO$_4$)$_3$ is blue-shifted from the emission of the related monomeric [(C^N^N)PtPPh$_3$]-

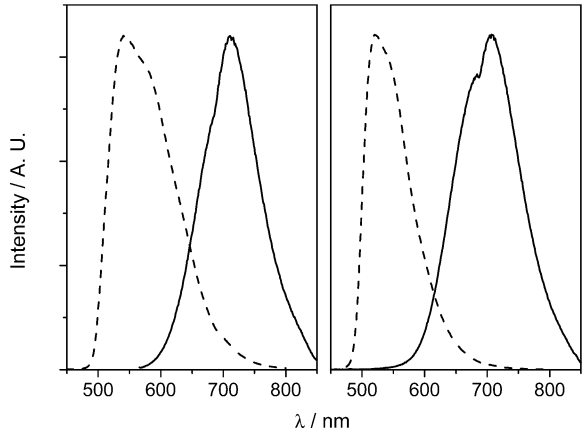

Figure 8. Normalized emission spectra of **7**$(ClO_4)_3$ (- - -) and **10**$(ClO_4)_3$ (—) in the solid state (left) and in acetonitrile solution (right) at 298 K (λ_{ex} 350 nm).

(ClO_4) ($\lambda_{max} \approx 560$ nm).[11b] Because the ^{3}IL emission of the Pd(II) analogue [(C^N^N)PdPPh$_3$](ClO_4) occurs at λ_{max} 480 nm,[23] we assign the 544 nm emission of the **7**$(ClO_4)_3$ solid to an excited state with mixed ^{3}MLCT and ^{3}IL parentage. The red emission (λ_{max} 630 nm) from the orange form of **10**$(BF_4)_3$ is comparable with the emission energy of the binuclear homologue [(C^N^N)$_2$Pt$_2$(μ-dppm)]$(ClO_4)_2$, which was previously assigned to a $^3(\pi\pi^*)$ excimeric emission with some ^{3}MMLCT character. This assignment coincides with the fact that only one close Pt···Pt contact (less than 3.5 Å) is revealed in the crystal structure of **10** (orange form) and the packing is dominated by intra- and intermolecular $\pi-\pi$ interactions. The deep red emissions from the red (λ_{max} 674 nm) and brown red (Figure 8, λ_{max} 709 nm) forms of **10**$(ClO_4)_3$ plus **17**$(ClO_4)_3$ (λ_{max} 710 nm) are seldom encountered in cyclometalated oligopyridyl Pt(II) complexes. Recently, we detected the ^{3}MMLCT emissions from concentrated solutions of [(C^N^N)Pt(isocyanide or carbonyl)]$^+$ salts at $\lambda_{max} \approx 700$ nm.[24] The emission from the yellow crystalline form of **10**$(ClO_4)_3$ cannot be accurately recorded due to the facile loss of solvated molecules. The emission energies of **7**$(ClO_4)_3$, **10**$(ClO_4)_3$, and **17**$(ClO_4)_3$ (Figure 8, λ_{max} 520, 710, and 710 nm, respectively) in acetonitrile at 298 K are similar to those in the solid state, thus indicating that comparable intramolecular configurations are maintained in both media. It is noteworthy that the emission maxima in acetonitrile at 298 K for the mono- and binuclear homologues of **10**$(ClO_4)_3$ and **17**$(ClO_4)_3$ occur at 535 and 652 nm [for **8**(ClO_4) and **9**$(ClO_4)_2$, respectively] and 655 nm [for binuclear **16**$(ClO_4)_2$],[11e] and thus the tendency of the emission energy to red-shift from mononuclear to linearly tethered bi- and trinuclear Pt(II) species is demonstrated.

The emission energy of **10**$(ClO_4)_3$ in acetonitrile at 298 K is concentration-dependent (see Supporting Information for spectra). With the increment of the complex concentration from 8.3 $\times 10^{-6}$ to 8.3 $\times 10^{-4}$ M, the emission maximum red-shifts from 670 to 710 nm. The excitation spectrum monitored at λ_{em} 710 nm shows a sharp peak at 560 nm, which is assigned to the ground-state aggregation of [(C^N^N)Pt]$^+$ units. Consistent with this, the well-defined low-energy absorption at ca. λ_{max} 500 nm

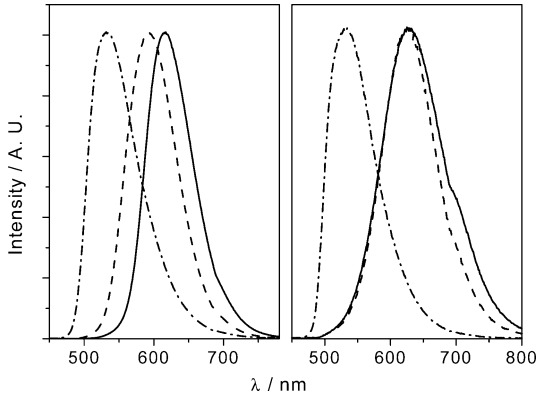

Figure 9. Normalized emission spectra of **12**(ClO_4) (- · -), **13**$(ClO_4)_2$ (- - -), and **14**$(ClO_4)_3$ (—) in the solid state (left) and in acetonitrile solution (right) at 298 K (λ_{ex} 350 nm).

in the excitation spectrum of [(C^N^N)PtC≡NCy](ClO_4) (λ_{em} 710 nm) was recently assigned to the ^{1}MMLCT transition.[24]

The emission of **10**$(ClO_4)_3$ in *n*-butyronitrile glass at 77 K is dependent on the excitation wavelength (see Supporting Information for spectra). Upon excitation at 360 nm, a structured emission at λ_{max} 510 nm with vibronic spacing of ~1290 cm^{-1} (lifetime ≈ 15 μs), together with a broad structureless emission at λ_{max} 633 nm (lifetime 6.6 μs), are observed. These two emission bands are tentatively assigned to the monomeric and excimeric $^3(\pi\pi^*)$ excited states, respectively. Upon excitation at 440 and 510 nm, structureless emission at λ_{max} 630 and 650 nm, respectively, is dominant. The site-selective emission of **10**$(ClO_4)_3$ implies the existence of multiple emissive species in the *n*-butyronitrile glassy medium, presumably due to varying degrees of aggregation of [(C^N^N)Pt]$^+$ lumophores. For **7**$(ClO_4)_3$ and **17**$(ClO_4)_3$, intense emission that is independent of complex concentration and excitation wavelength is observed at λ_{max} 520 and 710 nm, respectively, in acetonitrile solution at 298 K.

The emission spectra for **12**(ClO_4), **13**$(ClO_4)_2$, and **14**$(ClO_4)_3$ in the solid state and in acetonitrile at 298 K are shown in Figure 9. The solid-state emission maximum is red-shifted from mono- (532 nm) to bi- (593 nm) and trinuclear (617 nm) complexes. All three complexes are highly emissive in fluid solution with emission maximum occurring at 532, 625, and 628 nm, respectively. Interestingly, the emission energies of the mononuclear species **12**(ClO_4) are identical in the solid state and in diluted solution, while a minimal red-shift of emission energy in CH_3CN is detected when the number of tethered [4,4′-^{t}Bu$_2$(C^N^N)Pt] fragments is increased from two to three.

The emission spectra for **18**(ClO_4), **19**$(ClO_4)_2$, and **20**$(ClO_4)_3$ in the solid state and in acetonitrile (for **18**(ClO_4) only) at 298 K are shown in the Supporting Information. It is notable that the emission maxima for the mono- (628 nm), bi- (662 nm), and trinuclear (648 nm) derivatives are comparable. Only **18**(ClO_4) in this series is emissive in fluid solutions with emission maximum at 562 nm, and this is red-shifted from that of [(C^N^N)PtPPh$_3$](ClO_4) (535 nm) and [4,4′-^{t}Bu$_2$(C^N^N)-PtPPh$_3$](ClO_4) (532 nm). Hence, the electron-withdrawing ethoxycarbonyl group on the 4-position of (C^N^N) may lead to ^{3}dd or ^{3}MLCT excited states that are lower in energy than the ^{3}IL state (with a greater energy gap).

For **21**(PF_6) and **22**$(PF_6)_2$, which bear a crown ether moiety at the 4-position of the (C^N^N) ligand, the emission maximum

(23) Lai, S. W.; Cheung, T. C.; Chan, M. C. W.; Cheung, K. K.; Peng, S. M.; Che, C. M. *Inorg. Chem.* **2000**, *39*, 255−262.
(24) Lai, S. W.; Lam, H. W.; Lu, W.; Cheung, K. K.; Che, C. M. *Organometallics* **2002**, *21*, 226−234.

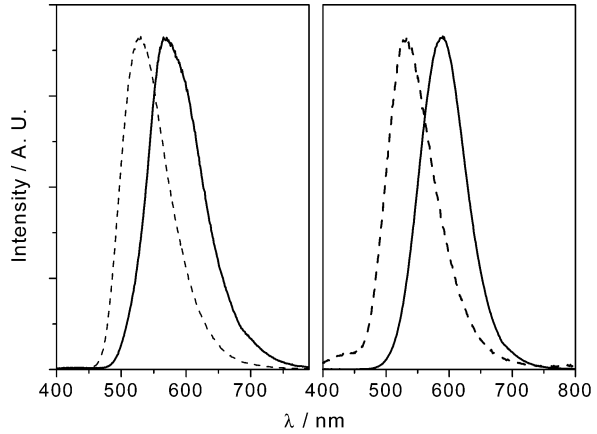

Figure 10. Normalized emission spectra of **21**(PF_6) (- - -) and **22**(PF_6)$_2$ (—) in the solid state (left) and in acetonitrile solution (right) at 298 K (λ_{ex} 350 nm).

(530 and 589 nm, respectively) recorded in acetonitrile solution approaches that in the solid state (530 and 570 nm, respectively), as shown in Figure 10. The emission energy of the monomeric species **21**(PF_6) is comparable to that of the [(C^N^N)PtPPh$_3$](ClO_4) and [4,4′-^{t}Bu$_2$(C^N^N)PtPPh$_3$](ClO_4) (**12**) congeners. Significantly, the fluid and solid-state emissions for the binuclear species **22**(PF_6)$_2$ are remarkably blue-shifted from those of the [(C^N^N)$_2$Pt$_2$(μ-dppm)](ClO_4)$_2$ (∼650 nm) and [{4,4′-^{t}Bu$_2$(C^N^N)}$_2$Pt$_2$(μ-dppm)](ClO_4)$_2$ (**13**) (∼625 nm) analogues, consistent with weaker Pt···Pt/$\pi-\pi$ interactions.

The emission spectra for crystalline forms of **23**(ClO_4), **24**(ClO_4)$_2$, and **25**(ClO_4)$_3$ at 298 K are shown in the Supporting Information. Clearly, the emission maximum red-shifts from mono- (613 nm) to tri- (627 nm) and binuclear (710 nm) derivatives. All three complexes are emissive in fluid solutions with λ_{max} occurring at 603, 629, and 657 nm for the mono-, bi-, and trinuclear species, respectively. The emission maximum of the mononuclear complex **23**(ClO_4) in this series is red-shifted from that for [(C^N^N)PtPPh$_3$](ClO_4) (535 nm), but λ_{max} for the trinuclear species is blue-shifted from that of [(C^N^N)$_3$Pt$_3$(μ_3-dpmp)](ClO_4)$_3$ (710 nm).

Spectroscopy of Palladium(II) Relatives. To gain further insight into the thienyl-substituted series, the spectroscopic properties of the Pd(II) congeners were investigated. Notably, the UV−vis spectra of the mononuclear **26**(ClO_4) and binuclear **27**(ClO_4)$_2$ in acetonitrile at 298 K feature comparable broad absorptions at λ_{max} 421 and 425 (sh) nm, respectively, and these are distinctly blue-shifted from the lowest-energy absorptions observed for the Pt_2 and Pt_3 analogues. The Pd(II) derivatives are emissive in alcoholic glassy solutions at 77 K (see Supporting Information for spectra) but not in the solid state or fluid solution. Complexes **26**(ClO_4) and **27**(ClO_4)$_2$ exhibit vibronically structured emission with λ_{max} (also λ_{0-0}) at 547 and 558 nm, respectively, and the former is blue-shifted by ca. 1900 cm^{-1} from the value (613 nm) recorded for the Pt analogue **23**(ClO_4) under the same conditions. The dpmp-supported Pd_2 derivative **11**(ClO_4)$_2$ is nonemissive in the solid state or in fluid solution.

Cyclic Voltammetry. The electrochemical data of selected Pt(II) complexes recorded in CH_3CN at 298 K are listed in Table 3. There is an irreversible oxidation wave at 1.00−1.36 V versus $Cp_2Fe^{+/0}$ for the Pt(II) complexes in this study. The cyclic voltammograms of the mononuclear Pt(II) complexes **12**(ClO_4), **18**(ClO_4), and **23**(ClO_4) in CH_3CN at 298 K exhibit a quasi-reversible reduction couple $E^{1/2}$ at −1.60, −1.26, and −1.47 V versus $Cp_2Fe^{+/0}$ respectively. Substitution at the 4-position of the (C^N^N) ligand has an effect upon these $E^{1/2}$ values; an electron-withdrawing ethoxycarbonyl group in **18**(ClO_4) shifts the first reduction wave to −1.26 V, while this reduction appears at −1.60 V for **12**(ClO_4) which bears two *tert*-butyl groups on the (C^N^N) ligand. The first reduction wave at −1.60 V for the Pd(II) derivative **26**(ClO_4) occurs at a more cathodic potential than that for the Pt(II) analogue **23**(ClO_4) (−1.47 V), indicating the extent of orbital mixing between the metal and cyclometalating ligand.

Table 3. Electrochemical Data[a] of Selected Pt(II) Complexes

complex	reduction $E^{1/2}$ (V)[b]	anodic peak E_{pa} (V)[b]
[(C^N^N)$_2$Pt$_2$(μ-dppm)](ClO_4)$_2$, (**9**)[c]	−1.23, −1.46	−
[(C^N^N)$_3$Pt$_3$(μ_3-dpmp)]$^{3+}$, (**10**)	−1.30, −1.46, −1.59	1.05
[4,4′-^{t}Bu$_2$(C^N^N)PtPPh$_3$]$^+$, (**12**)	−1.62	−
[{4,4′-^{t}Bu$_2$(C^N^N)}$_2$Pt$_2$(μ-dppm)]$^{2+}$, (**13**)	−1.49, −1.78	1.05
[{4,4′-^{t}Bu$_2$(C^N^N)}$_3$Pt$_3$(μ_3-dpmp)]$^{3+}$, (**14**)	−1.50, −1.77, −2.10	1.09
[{4-(4-MeOC$_6$H$_4$)(C^N^N)}$_3$Pt$_3$(μ_3-dpmp)]$^{3+}$, (**17**)	−1.51, −1.64, −1.90	1.00
[4-EtO$_2$C(C^N^N)PtPPh$_3$]$^+$, (**18**)	−1.26, −1.81	1.36
[{4-EtO$_2$C(C^N^N)}$_2$Pt$_2$(μ-dppm)]$^{2+}$, (**19**)	−1.07, −1.30, −2.04	1.10
[{4-EtO$_2$C(C^N^N)}$_3$Pt$_3$(μ_3-dpmp)]$^{3+}$, (**20**)	−1.03, −1.18, −1.42	1.13
[(S^N^N)PtPPh$_3$]$^+$, (**23**)	−1.47, −2.02	1.17
[(S^N^N)$_2$Pt$_2$(μ-dppm)]$^{2+}$, (**24**)	−1.29, −1.54	1.10
[(S^N^N)$_3$Pt$_3$(μ_3-dpmp)]$^{3+}$, (**25**)	−1.21, −1.41, −1.59	1.12
[(S^N^N)PdPPh$_3$]$^+$, (**26**)	−1.60, −1.90	1.19
[(S^N^N)$_2$Pd$_2$(μ-dppm)]$^{2+}$, (**27**)	−1.46, −1.64, −1.90	1.29

[a] Determined in CH_3CN at 298 K with 0.1 M ^{n}Bu$_4$NPF$_6$ as supporting electrolyte; scanning rate: 50 mV s^{-1}. [b] Values versus $E^{1/2}$ ($Cp_2Fe^{+/0}$) [0.04−0.05 V vs $Ag/AgNO_3$ (0.1 M in CH_3CN) reference electrode]. [c] Values taken from ref 11e.

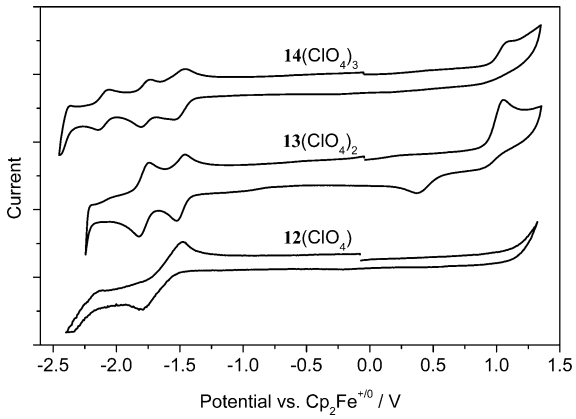

Figure 11. Cyclic voltammograms of **12**(ClO_4), **13**(ClO_4)$_2$, and **14**(ClO_4)$_3$ in acetonitrile at 298 K (with 0.1 M ^{n}Bu$_4$NPF$_6$ as supporting electrolyte; scanning rate: 50 mV s^{-1}).

Upon going from mono- to bi- and trinuclear complexes, the first reduction wave(s) based at the cyclometalating ligand(s) is found to split into two and three couples, respectively, as shown in Figure 11 for the [4,4′-^{t}Bu$_2$(C^N^N)Pt] series (see Supporting Information for other analogues). For example, the reduction waves are observed at −1.62, −1.49/−1.78, and −1.50/−1.77/−2.10 V for the mono-, bi-, and trinuclear species, respectively, in the [4,4′-^{t}Bu$_2$(C^N^N)Pt] series; −1.26, −1.07/−1.30, and −1.03/−1.18/−1.42 V in the [4-EtO$_2$C(C^N^N)Pt]

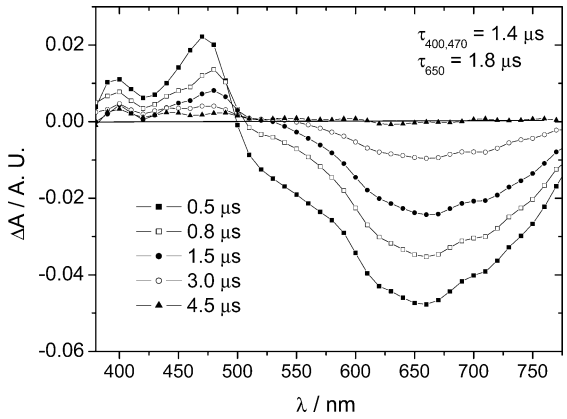

Figure 12. Time-resolved difference absorption spectra of **14**$(ClO_4)_3$ in CH_3CN at 298 K.

series; and −1.47, −1.29/−1.54, and −1.21/−1.41/−1.59 V in the [(S^N^N)Pt] series. This indicates that the cyclometalating ligands in the bi- and trinuclear complexes are inequivalent upon sequential reduction.

Photophysical and Electrochemical Studies on [{4,4′-^{t}Bu$_2$-(C^N^N)}$_3$Pt$_3$(μ_3-dpmp)](ClO$_4$)$_3$, 14(ClO$_4$)$_3$. Complex **14**$(ClO_4)_3$, which bears two *tert*-butyl substituents on each (C^N^N) ligand, displays superior solubility in a variety of organic solvents and was chosen as an illustrative example to test the effects of solvent on the absorption and emission properties (see Supporting Information for spectra). The effect of solvent polarity on the absorption is minimal. The emission maximum (lifetime, quantum yield) changes from 621 (2.7 μs, 0.18) to 628 (1.7 μs, 0.08), 631 (2.3 μs, 0.15), and 649 (0.6 μs, 0.05) nm when the solvent is changed from benzene to CH_3CN, CH_2Cl_2, and EtOH.

To characterize the photophysical nature of these Pt_3 lumophores in detail, the time-resolved difference absorption (TA) spectra of **14**$(ClO_4)_3$ in CH_3CN were recorded (Figure 12). The decay of the absorption signals (1.4−1.8 μs) matched the emission lifetime (1.7 μs), which is in accordance with the absorption originating from the emissive excited state. The salient features in the TA spectra are intense luminescence bleaching in the 500−775 nm range and strong absorption in the 380−500 nm range (with λ_{max} ca. 400 and 470 nm).

By employing the electrochemical data plus the spectroscopic measurements, it is possible to estimate the excited-state potential of **14**$(ClO_4)_3$ by using the following equation: $E(*\mathbf{14}^{3+}/\mathbf{14}^{2+}) = E(\mathbf{14}^{3+}/\mathbf{14}^{2+}) + E_{0-0}(\mathbf{14}^{3+})$. The cyclic voltammogram of **14**$(ClO_4)_3$ reveals the first quasi-reversible one-electron reduction wave [$E(\mathbf{14}^{3+}/\mathbf{14}^{2+})$, $(i_{pc}/i_{pa}) \approx 1$] at −1.50 V versus $Cp_2Fe^{+/0}$ (−1.10 V vs NHE) in acetonitrile. The 0−0 transition energy of $\mathbf{14}^{3+}$, $E_{0-0}(\mathbf{14}^{3+})$, can be estimated from the overlap of the emission and excitation spectra, which occurs at 2.4 eV. Thus, $E(*\mathbf{14}^{3+}/\mathbf{14}^{2+})$ is estimated to be ca. 0.9 V versus $Cp_2Fe^{+/0}$ (1.3 V vs NHE), which signifies that $*\mathbf{14}^{3+}$ is a strong photooxidant. This value is slightly smaller than that previously calculated for $E(*\mathbf{9}^{2+}/\mathbf{9}^{+})$ [1.61 V vs NHE].[11e]

Complex **14**$(ClO_4)_3$ was chosen to investigate the electroluminescent properties of positively charged Pt(II)-based triplet lumophores in light-emitting devices. Thus, **14**$(ClO_4)_3$ was spin-coated onto ITO glass to give a film with a thickness of ca. 0.1 μm, and an aluminum electrode was vacuum-deposited onto this cast film. Preliminary results (see Supporting Information for plots) show that the single-layer device displays orange-red emission under a forward bias, with maximum luminance levels of 10 cd m^{-2} at a current density of ca. 2.2 mA cm^{-2}. No emission was observed in the reverse bias, although the negative current was recorded. The electroluminescence maximum of ca. 634 nm is close in energy to the fluid and solid-state photoluminescence of **14**$(ClO_4)_3$, indicating the same origin for the electro- and photoluminescence. The low turn-on voltage (< 3.0 V), relatively long response time (ca. 10 s at 6 V), and measurable reverse current suggest an electrochemical mechanism instead of diode-like for this light-emitting device.[25] The poor performance is presumably due to an irreversible one-electron oxidation process.

Discussion

Weak Intra- and Intermolecular Interactions. The salient features in the crystal structures of the tethered oligopyridine cyclometalated Pt(II) complexes are the intramolecular Pt···Pt contacts and intra- and intermolecular $\pi-\pi$ interactions. Table 4 has been compiled to facilitate comparison between the literature-reported data and the present work. Three parameters, Pt···Pt distance, torsion angle between the Pt(II) coordination planes, and Pt···Pt···Pt angle (for trinuclear species), have been selected to characterize and illustrate these interactions. Generally, shorter Pt···Pt distances are accompanied by a larger torsion angle between the ligated Pt(II) planes. The optimized configuration for face-to-face π-stacking interactions between two aromatic planes is staggered (i.e., torsion angle significantly larger than 0°),[26] whereas face-to-face π overlap in an eclipsed fashion (i.e., torsion angle ca. 0°) introduces repulsive forces. However, the stabilization effect of Pt···Pt contacts in these tethered complexes apparently overcomes this repulsion between the ligated Pt(II) moieties, and all Pt_3 complexes adopt a *syn,syn*-configuration. The partially staggered geometry observed is in essence the compromise between Pt···Pt attraction(s) and repulsion induced by unfavorable π-stacking interactions. A consequence of this compromise is that the Pt···Pt···Pt chains in the tethered Pt(II) complexes in this study deviate from linearity, as shown by the intramolecular Pt···Pt···Pt angles of 162 ± 7°. The "ideal" combination of Pt···Pt and $\pi-\pi$ interactions can apparently be achieved in oligomers of untethered Pt(II) complexes through self-assembly, as is reported for the green form of [(tpy)Pt(C≡C−C≡CH)](CF_3SO_3),[9f] where the Pt···Pt distance is 3.388 Å, the torsion angle is 134.4°, and the Pt···Pt···Pt angle is 179°. The intriguing coiled chains observed in the crystal packing of the trinuclear complex **20**$(ClO_4)_3 \cdot 2CH_3CN$ can be rationalized by a combination of intramolecular Pt···Pt and intermolecular $\pi-\pi$ interactions. We note that trinuclear Pd(II) counterparts have not been prepared or isolated; Pd···Pd interactions are considerably weaker and presumably cannot compete with π-stacking interactions.

When crown ether units are introduced into this system, the observed trend for Pt···Pt distances and torsion angles can be broken. As listed in Table 4, the Pt···Pt distance in **22** is 3.827 Å, which is considerably larger than that in [(C^N^N)$_2$Pt$_2$(μ-dppm)](ClO$_4$)$_2$,[11e] even though the torsion angle is comparable

(25) (a) Lee, J. K.; Yoo, D. S.; Handy, E. S.; Rubner, M. F. *Appl. Phys. Lett.* **1996**, *69*, 1686−1688. (b) Buda, M.; Kalyuzhny, G.; Bard, A. J. *J. Am. Chem. Soc.* **2002**, *124*, 6090−6098. (c) Welter, S.; Brunner, K.; Hofstraat, J. W.; De Cola, L. *Nature* **2003**, *421*, 54−57.
(26) Hunter, C. A.; Sanders, J. K. M. *J. Am. Chem. Soc.* **1990**, *112*, 5525−5534.

Table 4. Selected Structural Parameters Concerning Pt···Pt Interactions in Tethered Oligopyridine Cyclometalated Pt(II) Complexes[a]

complex	Pt···Pt distance/Å	torsion angle/deg	Pt···Pt···Pt angle/deg	ref
$[(tpy)_2Pt_2(\mu\text{-can})]^{3+}$	2.998	21		31
$[(tpy)_2Pt_2(\mu\text{-gua})]^{3+}$	3.090; 3.071	28.6; 22.1		32
$[(tpy)_2Pt_2(\mu\text{-pz})]^{3+}$	3.432			33
$[(tpy)_2Pt_2(\mu\text{-az})]^{3+}$	3.13			34
$[(tpy)_2Pt_2(\mu\text{-dpf})]^{3+}$	3.049			34
$[(tpy)_2Pt_2(\mu\text{-SNS})]^{2+}$	3.908	14		35
$[(C\text{^}N\text{^}N)_2Pt_2(\mu\text{-pz})]^{+}$	3.612			11e
$[(C\text{^}N\text{^}N)_2Pt_2(\mu\text{-dppm})]^{2+}$ (**9**)	3.270	44.6		11b
$[\{4\text{-}(4\text{-}ClC_6H_4)\text{-}(C\text{^}N\text{^}N)\}_2Pt_2(\mu\text{-dppm})]^{2+}$	3.150	27.2		36
$[\{4\text{-}(4\text{-}MeC_6H_4)\text{-}(C\text{^}N\text{^}N)\}_2Pt_2(\mu\text{-dppm})]^{2+}$	3.245	20.7		11e
$[\{4\text{-(aza-15-crown-5)-}(C\text{^}N\text{^}N)\}_2Pt_2(\mu\text{-dppm})]^{2+}$ (**22**)	3.827	43.2		this work
$[(S\text{^}N\text{^}N)_2Pt_2(\mu\text{-dppm})]^{2+}$ (**24**)	3.321	29.0		this work
$[(C\text{^}N\text{^}N)_3Pt_3(\mu_3\text{-dpmp})]^{3+}$ (**10**, red form)	3.194; 3.399	26.3; 15.5	169	this work
$[(C\text{^}N\text{^}N)_3Pt_3(\mu_3\text{-dpmp})]^{3+}$ (**10**, orange form)	3.364; 3.617	34.6; 4.7	162	this work
$[\{4,4'\text{-}{}^t\!Bu_2(C\text{^}N\text{^}N)\}_3Pt_3(\mu_3\text{-dpmp})]^{3+}$ (**14**)	3.217; 3.601	29.6; 9.3	157	this work
$[\{4\text{-}EtO_2C(C\text{^}N\text{^}N)\}_3Pt_3(\mu_3\text{-dpmp})]^{3+}$ (**20**)	3.466; 3.647	33.7; 8.9	162	this work
$[(S\text{^}N\text{^}N)_3Pt_3(\mu_3\text{-dpmp})]^{3+}$ (**25**)	3.254; 3.389	33.0; 18.7	163	this work
[Bosnich's Pt_2 receptor: $Pt(salap)NH_3]^{2+}$	3.262; 3.303		173	15a
$[(tpy)Pt(C{\equiv}C{-}C{\equiv}CH)]^{+}$ (green form)	3.388	134.4	179	9f
$[(tpy)Pt(C{\equiv}C{-}C{\equiv}CH)]^{+}$ (red form)	3.394; 3.648	49.7; 57.1	154	9f

[a] Hgua = guanidine; Hpz = pyrazole; Haz = azaindole; Hdpf = diphenylformamidine; Hcan = arginine; H_2SNS = dithiouracil; H_2salap = 2-salicylideneaminophenol.

(43.2° versus 44.6°). It is apparent that the C−H···O interactions between H3 on the 4′-position of one diimine ligand and the oxygen atoms (O2−O4) on the adjacent [4-(aza-15-crown-5)-(C^N^N)Pt]$^+$ fragment are more important than the intramolecular Pt···Pt interaction in terms of their impact upon the crystal packing. No Pt···Pt interaction is expected in fluid solutions, because the emission maximum (589 nm) recorded in acetonitrile solution is comparable to that in the solid state (570 nm). It is noteworthy that interactions of crown ethers with alkaline and alkaline earth metal and ammonium ions are ubiquitous but the binding of a C−H group to a crown ether moiety is comparatively rare.

MMLCT Transition in Electronic Spectroscopy. The MMLCT excited states in Pt(II) complexes have attracted considerable attention since the early works by the Yersin and Miskowski groups.[6] Previous studies by Che and co-workers on binuclear derivatives bearing cyclometalated 6-phenyl-2,2′-bipyridine, $[(C\text{^}N\text{^}N)_2Pt_2(\mu\text{-L})]^{n+}$ (L = pyrazole, dppm), revealed interesting photophysical properties, including distinctive low-energy emissions in fluid solutions.[11e] However, assignment of these low-energy emissions to ^{3}MMLCT excited states is complicated by the fact that the corresponding excimeric $\pi\pi^*$ emissions occur in a similar spectral region. We envisaged that the tethered trinuclear Pt(II) complexes in the present study would enable us to elucidate the impact of metal···metal and $\pi-\pi$ interactions upon MMLCT excited states.

The emission maxima of the [4,4′-^{t}Bu$_2$(C^N^N)Pt] and [4-(aza-15-crown-5)(C^N^N)Pt] series of complexes in acetonitrile solution at 298 K are virtually identical to their respective values in the solid state; therefore, the extent of intramolecular Pt···Pt and $\pi-\pi$ interactions revealed in their crystal structures is likely to be maintained in fluid solutions, assuming that the emissions are directly related to these weak noncovalent interactions. The difference between the absorption spectra of these complexes can shed light on the net effect of extending from mononuclear to tethered bi- and trinuclear Pt(II) homologues. The corrected absorption difference spectrum (Figure 6, inset) between **12**(ClO_4) and **14**$(ClO_4)_3$ in acetonitrile at 298 K features a broad low-energy band with a maximum at 422 nm ($\epsilon \approx 4000$ dm^3 mol^{-1} cm^{-1}); this is apparently derived from ground-state Pt···Pt interaction, and the inhomogeneous broadening presumably arises from the changeability of the Pt···Pt separation in solution. The corrected absorption difference spectrum (Figure 7, inset) between **21**(PF_6) and **22**$(PF_6)_2$ in acetonitrile at 298 K features a broad low-energy band with a maximum at 430 nm ($\epsilon \approx 3000$ dm^3 mol^{-1} cm^{-1}). As noted in the crystal structures, there is no Pt···Pt interaction in **22**$(PF_6)_2$ due partly to the influence of the crown ether moieties, but **14**$(ClO_4)_3$ may contain short Pt···Pt contacts. Therefore, the low-energy band at λ_{max} 430 nm is tentatively assigned to the ground-state aggregation of the lumophores in **22** through intramolecular $\pi-\pi$ interaction.

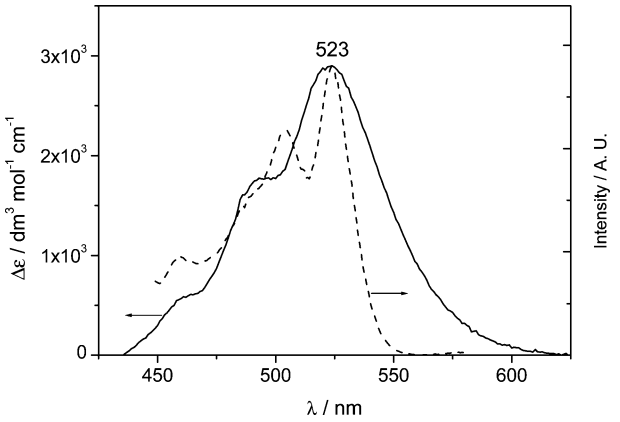

Figure 13. Plot of $\Delta\epsilon$ versus wavelength (—) for **10**$(ClO_4)_3$ and **14**$(ClO_4)_3$ in acetonitrile at 298 K, and excitation spectrum (- - -) of **10**$(ClO_4)_3$ in MeOH/EtOH (1/4, v/v) at 77 K (monitored at λ_{em} 677 nm, complex concentration $\sim 1 \times 10^{-5}$ mol dm^{-3}).

A stark observation is apparent when the absorption difference spectrum between **10**$(ClO_4)_3$ and **14**$(ClO_4)_3$ in acetonitrile at 298 K (Figure 13) is scrutinized. This spectrum features a well-structured low-energy band at 523 nm (peak maximum) with ϵ and vibronic progression of $\sim$3000 dm^3 mol^{-1} cm^{-1} and 1080 cm^{-1}, respectively (the vibronic progression may correspond to the excited-state aromatic ring deformation). The energy and vibronic progression coincide with the corresponding values in

the excitation spectrum of **10**$(ClO_4)_3$ in MeOH/EtOH (1/4, v/v) at 77 K (monitored at λ_{em} 677 nm), as shown in Figure 13. Furthermore, the energy of this band is comparable to that of the 500 nm band in the excitation spectrum of [(C^N^N)PtC≡NCy](ClO_4) (concentration $\sim 7 \times 10^{-3}$ mol dm^{-3}) in acetonitrile at 298 K when monitored at 710 nm, and the latter was ascribed to a MMLCT transition.[24] Hence, we propose that the absorption band at λ_{max} 523 nm, derived from the absorption difference spectra, can be considered as a distinct singlet MMLCT transition and corresponds to the low-energy ^{3}MMLCT emission at $\lambda_{max} \approx 700$ nm for **10**$(ClO_4)_3$ in fluid solutions and the solid state. In view of the fact that there are two Pt···Pt contacts in the crystal structure of **10**$(ClO_4)_3$, but only one in **14**$(ClO_4)_3$, the 523 nm band in the absorption difference spectrum can be tentatively attributed to the net effect of one Pt···Pt interaction (note that in this case the interligand effect has been off-set). Significantly, Bosnich and co-workers recently proposed that the presence of an absorption band beyond 500 nm ($\epsilon \approx 1500$ dm^3 mol^{-1} cm^{-1}) can be similarly attributed to the association of a Pt_2 terpyridine molecular receptor with neutral and anionic Pt-based guests through Pt···Pt interactions.[15a]

Tuning of the Emission Energy. To obtain cyclometalated Pt(II) complexes that display lower emission energies in fluid solution, two strategies could be employed. The first is the introduction of electron-withdrawing groups on the cyclometalating moiety (or electron-donating substituents on the ancillary ligands), assuming that the emissions are MLCT in nature and the cyclometalated ligand is the electron acceptor upon photoexcitation. However, this approach is limited by the energy gap law, which states that low emission energy for a charge-transfer excited state correlates to low quantum yield and short lifetime. The second method, which can lead to high-efficiency low-energy Pt(II) emitters, is to connect discrete lumophore units into multinuclear species through Pt···Pt and $\pi-\pi$ interactions. In solution, the Pt···Pt/$\pi-\pi$ contacts would be locked into place by judiciously chosen oligophosphine ligands, which tether the lumophore units in a face-to-face linear conformation to afford highly emissive MMLCT excited states.

The tuning of the emission energies from mono- to bi- and trinuclear cyclometalated complexes has been demonstrated; for example, the emission maxima for the [(C^N^N)Pt] series in CH_3CN solution are 560, 650, and 710 nm, respectively. However, for all of the linearly tethered trinuclear complexes, the emission energies appear in the λ_{max} 657−710 nm range (in acetonitrile solutions at 298 K), and further red-shifted emissions from these MMLCT excited states have not thus far been achieved through ligand modification. There may be a fundamental limitation for the tethering approach; that is, the conflict between close intramolecular Pt···Pt attraction and $\pi-\pi$ repulsion of adjacent [(C^N^N)Pt] moieties in an eclipsed or staggered manner can prevent a more intimate approach between Pt(II) centers. Nevertheless, further extension of the tethered series of cyclometalated Pt(II) complexes to tetranuclear and higher homologues can be envisaged.

Summary

Control over the absorption and emission energies of multinuclear cyclometalated Pt(II) complexes has been achieved by modifying the shape and chelating directionality of the tethering oligophosphine ligand. For "linear" Pt_3 species, the allowed charge-transfer bands cover the visible spectrum. Hence, these molecular materials may find applications in dye-sensitized solar-energy cells and light-emitting electrochemical cells (LECs), like the red LEC demonstrated in this work, although the efficiency of the device clearly requires considerable improvement. The NIR emissions from these lumophores are ideal signal outputs for biomolecular probes and chemosensors. The nature of the excited states, which are extremely sensitive to the microenvironment, have been probed and subsequently assigned. Evidence from the present study indicates that both the ground and excited states of the higher homologues of this class of luminescent Pt(II) complexes can readily engaged in weak noncovalent interactions such as d^8-d^8 contacts, $\pi-\pi$ stacking, and C−H···O hydrogen bonding.

Experimental Section

Materials and General Procedures. All starting materials were purchased from commercial sources and used as received unless stated otherwise. The solvents used for synthesis were of analytical grade. The compounds 3-(2-pyridyl)-5-phenyl-1,2,4-triazine,[27] 4-hydroxycarbonyl-6-phenyl-2,2′-bipyridine,[28] bis(diphenylphosphinomethyl)phenylphosphine (dpmp),[22] [(C^N^N)PtCl],[29] [(C^N^N)PdCl],[29] [4-(4-$MeOC_6H_4$)(C^N^N)PtCl],[24] [(S^N^N)PtCl],[30] and [(S^N^N)PdCl][30] were prepared according to literature methods. ^{1}H, ^{13}C, ^{31}P, and ^{195}Pt NMR spectra were recorded on a Bruker DRX 500, Avance 400, or DRX 300 FT-NMR spectrometer with TMS (^{1}H and ^{13}C), H_3PO_4 (^{31}P), and H_2PtCl_6 (^{195}Pt) as references. Mass spectra (FAB) were obtained on a Finnigan MAT 95 mass spectrometer. Elemental analyses were performed by Beijing Institute of Chemistry, Chinese Academy of Sciences. Details of solvent treatment for photophysical studies and cyclic voltammetric studies have been described earlier.[11e] UV−vis spectra were recorded on a Perkin-Elmer Lambda 19 UV/vis spectrophotometer. Solution samples for emission and time-resolved difference absorption measurements were degassed by at least four freeze−pump−thaw cycles. Emission spectra were obtained on a SPEX Fluorolog-2 model F111 fluorescence spectrophotometer. Emission lifetime measurements were performed with a Quanta Ray DCR-3 pulsed Nd:YAG laser system (pulse output 355 nm, 8 ns). Luminescent quantum yields were referenced to [Ru(bpy)$_3$]$(ClO_4)_2$ in acetonitrile ($\phi = 0.062$) (estimated error ±15%). Time-resolved difference absorption experiments were performed with the above-mentioned Nd:YAG laser system. The monitoring light was from a 300 W continuous wave tungsten−halogen or xenon lamp oriented orthogonally to the direction of the laser pulse. Transient species were monitored by monochromatic light from a tungsten or xenon lamp. The difference absorption signals at individual wavelengths were fed to the Tektronix 2430 or TDS 350 oscilloscope. The entire optical difference spectrum was generated point to point by monitoring at each wavelength. Details of cyclic voltammetric studies have been described earlier.[12a]

General Procedure for Syntheses of Phosphine-Ligated Complexes. (Caution! *Perchlorate salts are potentially explosive and should*

(27) Culbertson, B. M.; Parr, G. R. *J. Heterocycl. Chem.* **1967**, *4*, 422−424.
(28) Neve, F.; Crispini, A.; Di Pietro, C.; Campagna, S. *Organometallics* **2002**, *21*, 3511−3518.
(29) Constable, E. C.; Henney, R. P. G.; Leese, T. A.; Tocher, D. A. *J. Chem. Soc., Chem. Commun.* **1990**, 513−515.
(30) Constable, E. C.; Henney, R. P. G.; Raithby, P. R.; Sousa, L. R. *J. Chem. Soc., Dalton Trans.* **1992**, 2251−2258.
(31) Ratilla, E. M. A.; Scott, B. K.; Moxness, M. S.; Kostić, N. M. *Inorg. Chem.* **1990**, *29*, 918−926.
(32) Yip, H. K.; Che, C. M.; Zhou, Z. Y.; Mak, T. C. W. *J. Chem. Soc., Chem. Commun.* **1992**, 1369−1371.
(33) Bailey, J. A.; Gray, H. B. *Acta Crystallogr.* **1992**, *C48*, 1420−1422.
(34) Bailey, J. A.; Miskowski, V. M.; Gray, H. B. *Acta Crystallogr.* **1993**, *C49*, 793−796.
(35) Tzeng, B. C.; Fu, W. F.; Che, C. M.; Chao, H. Y.; Cheung, K. K.; Peng, S. M. *J. Chem. Soc., Dalton Trans.* **1999**, 1017−1023.
(36) Wu, L. Z.; Cheung, T. C.; Che, C. M.; Cheung, K. K.; Lam, M. H. W. *Chem. Commun.* **1998**, 1127−1128.

be handled with care and in small amounts.) A mixture of [R^x(C^N^N)-MCl] (M = Pt or Pd) and the phosphine ligand in CH_2Cl_2/CH_3OH (1/5, v/v) was stirred for 12 h at room temperature. The resulted clear solution was filtered into a saturated CH_3OH solution of $LiClO_4$ (or Et_4NBF_4, NH_4PF_6). After the volume of the mixture was reduced to about 5 mL, Et_2O (100 mL) was added to precipitate the product, which was collected on sinter glass and washed with H_2O/CH_3OH and Et_2O, then recrystallized from CH_3CN/Et_2O unless otherwise stated.

The syntheses and characterization data of all new ligands and complexes are provided in the Supporting Information.

X-ray Crystallography. Single crystals of **10**$(ClO_4)_3 \cdot H_2O$ (red form: slow diffusion of benzene vapor into a CH_3CN solution), **6**, **9**$(ClO_4)_3$, **10**$(ClO_4)_3 \cdot 2Et_2O \cdot CH_3CN$ (orange form), **14**$(ClO_4)_3 \cdot 3CH_3CN$, **20**$(ClO_4)_3 \cdot 2CH_3CN$, **22**$(PF_6)_2$, **24**$(ClO_4)_2 \cdot 2CH_3CN$, and **25**$(ClO_4)_3 \cdot 1.5Et_2O \cdot CH_3CN$ (slow diffusion of Et_2O into CH_3CN solutions) were obtained. For **14**$(ClO_4)_3 \cdot 3CH_3CN$, one crystallographic asymmetric unit consists of one formula unit, including three anions and three acetonitrile solvent molecules. Three ClO_4^- anions were located at four positions. The anion containing Cl3 was located at the special position, while the anion containing Cl4 was considered to have half occupancy. One of the *tert*-butyl group was disordered into two sets of positions, in the mode of rotation along C−C bond. For convergence of least-squares refinement, restraints were applied assuming similar C−C and O···C bond lengths, respectively. For **20**$(ClO_4)_3 \cdot 2CH_3CN$, one crystallographic asymmetric unit consists of one formula unit, including three anions and two acetonitrile solvent molecules. The CH_3 group of the central ethoxyl group is disordered into two positions, and restraints were applied assuming similar C−C and O···C bond lengths or distances for the disordered C atoms, respectively. For **6**, one crystallographic asymmetric unit consists of one formula unit. In the final stage of least-squares refinement, only Pt and Cl atoms were refined anisotropically, and the other non-hydrogen atoms were refined isotropically. For **22**$(PF_6)_2$, one crystallographic asymmetric unit consists of half of one formula unit, including one anion located in two sets of positions (each with half occupancy). One of the anions was disordered in the mode of sharing three F atoms for two parts, due to its closeness to the special position; restraints were applied to the disordered anion assuming similar P−F bond lengths. The end-side of the crown ether fragments showed high displacement parameters, so restraints were also applied assuming similar O−C, C−C, and 1,3-O···C bond lengths or distances, respectively. In the final stage of least-squares refinement, the F atoms of the disordered anion and 8 non-H atoms of the crown ether end-side were refined isotropically, and the remaining non-hydrogen atoms were refined anisotropically. For **24**$(ClO_4)_2 \cdot 2CH_3CN$, one crystallographic asymmetric unit consists of one and a half formula unit, including one anion (in two positions) and one CH_3CN solvent molecule. For **25**$(ClO_4)_3 \cdot 1.5Et_2O \cdot CH_3CN$, one crystallographic asymmetric unit consists of one formula unit, including three anion, one CH_3CN, and one and a half Et_2O solvent molecules. In the final stage of least-squares refinement, the O atoms of ClO_4^- and atoms of solvate molecules were refined isotropically, and the other non-hydrogen atoms were refined anisotropically.

Acknowledgment. We are grateful for financial support from The University of Hong Kong, the Research Grants Council of Hong Kong SAR, China [HKU 7039/03P], and the Croucher Foundation of Hong Kong. We thank the reviewers for helpful comments.

Supporting Information Available: Crystal data (CIF); synthetic and characterization data; supplementary UV−vis absorption, emission spectra, and cyclic voltammograms; scheme of ligand synthesis. This material is available free of charge via the Internet at http://pubs.acs.org.

JA039727O